GEOLOGICA CARPATHICA, 2026, 77, 1, 65–91 https://doi.org/10.31577/GeolCarp.2026.04

Tectonostratigraphic evolution of the Cretaceous–Paleogene Dinaric foreland basin in eastern Herzegovina

MARIJA BJELOGRLIĆ[1,2,✉], MARINKO TOLJIĆ[1], BOJAN GLAVAŠ-TRBIĆ[2], STJEPAN ĆORIĆ[3], BORNA LUŽAR-OBERITER[4], VIOLETA GAJIĆ[1] and ROBERT ŠAMARIJA[5]

[1]University of Belgrade, Faculty of Mining and Geology, Djušina 7, 11000 Belgrade, Serbia
[2]Geological Survey of Serbia, Rovinjska 12, 11000 Belgrade, Serbia
[3]GeoSphere Austria, Neulinggasse 38, 1030 Vienna, Austria
[4]University of Zagreb, Faculty of Science, Horvatovac 102B, 10000 Zagreb, Croatia
[5]Institute of Applied Geosciences, Karlsruhe Institute of Technology, Adenauerring 20a, 76131, Karlsruhe, Germany

(Manuscript received August 13, 2025; accepted in revised form February 16, 2026; Associate Editor: Rastislav Vojtko)

Abstract: The Bosnian Flysch, deposited within the Dinaric foreland basin in eastern Herzegovina, consists of thick deep-sea turbiditic successions represented by the Lower Cretaceous Vranduk Formation and the Upper Cretaceous–Paleogene Ugar Formation. The Vranduk Formation in eastern Herzegovina is predominantly siliciclastic in nature, sourced from the northeasterly positioned Adria-derived continental basement units and Neotethys ophiolites. Biostratigraphic data suggest a Barremian to Albian age for the Vranduk Formation in this area. The Ugar Formation in eastern Herzegovina consists of three members: (i) basal Upper Cretaceous limestone breccias and conglomerates; (ii) Upper Cretaceous carbonate–clastic sediments; and (iii) Paleocene carbonate–siliciclastic sediments, derived from the SW situated Adriatic Carbonate Platform, and redeposited into the foreland basin. Our biostratigraphic data indicate a Turonian to Lower Santonian age for the basal breccias and conglomerates, an Upper Santonian to Maastrichtian age for the Upper Cretaceous carbonates, and a Paleocene age for the carbonate–clastic sediments. Kinematic analysis of faults and the reconstruction of paleostress fields have identified three significant and temporally distinct tectonic phases. Reverse and strike-slip faults were active during the Cretaceous–Paleogene deformation phase, which developed under compression of a general NE–SW orientation. The second deformation is characterized by a regional event, the Oligocene–Miocene extension, during which older reverse structures were reactivated as normal faults, and new normal faults were also developed. Here, normal faults active in extension parallel to the orogen (NW–SE orientation) and those active in extension perpendicular to the orogen (NE–SW orientation) can be distinguished. The youngest, Late Miocene deformation phase is documented by a group of faults active in compression that affected the entire Dinarides. This stress field was characterized by reverse and strike-slip faults active in N–S oriented compression.

Keywords: Vranduk Formation, Ugar Formation, biostratigraphy, tectonic evolution, foreland basin, eastern Herzegovina

Introduction

Foreland basins (Fig. 1a) commonly develop in orogenic belts as a result of long-lasting thrusting and progressive deformation, leading to crustal thickening and orogenic uplift. Compressional tectonics initiates foreland basin development and progressive migration of an orogenic fold-and-thrust belt toward the continental interior (Matenco et al. 2010). The resulting thrust sheets impose a tectonic load on the lithosphere, causing its flexural bending. This process leads to the formation of a foreland basin, which is subsequently infilled with clastic material eroded from the orogenic hinterland (Lyon-Caen & Molnar 1985; Flemings & Jordan 1990; DeCelles & Giles 1996).

Foreland basins are typically asymmetric, extending from the orogenic front toward the continental interior. They reach their maximum depth along the orogenic margin and gradually become shallower away from the mountain belt. These basins generally comprise four principal depositional zones: the wedge-top, foredeep, forebulge, and backbulge (DeCelles & Giles 1996). Late-stage accretion of synorogenic deposits often complicates the distinction between sediments originally deposited in front of the orogen and those that were later incorporated into the orogenic system and tectonically transported by thrusting and deformation (Poblet & Lisle 2011; Balling et al. 2021).

As collisional processes advance, foreland basin systems evolve from an underfilled flysch stage to an overfilled molasse stage (Sinclair 1997a, b). The early flysch stage is characterized by limited sediment supply and pronounced subsidence, resulting in deep water sedimentation concentrated near the orogenic front under increasingly deep-water conditions (Lužar-Oberiter et al. 2023). Continued orogenic uplift enhances clastic supply, leading to increased depositional diversity within the basin (Babić & Zupanič 2008; Toljić et al. 2018; Lužar-Oberiter et al. 2023).

The Dinaric orogen developed through long-term Neotethyan convergence, as a result of Late Jurassic ophiolite

✉ corresponding author: Marija Bjelogrlić
G804-23@dok.rgf.bg.ac.rs

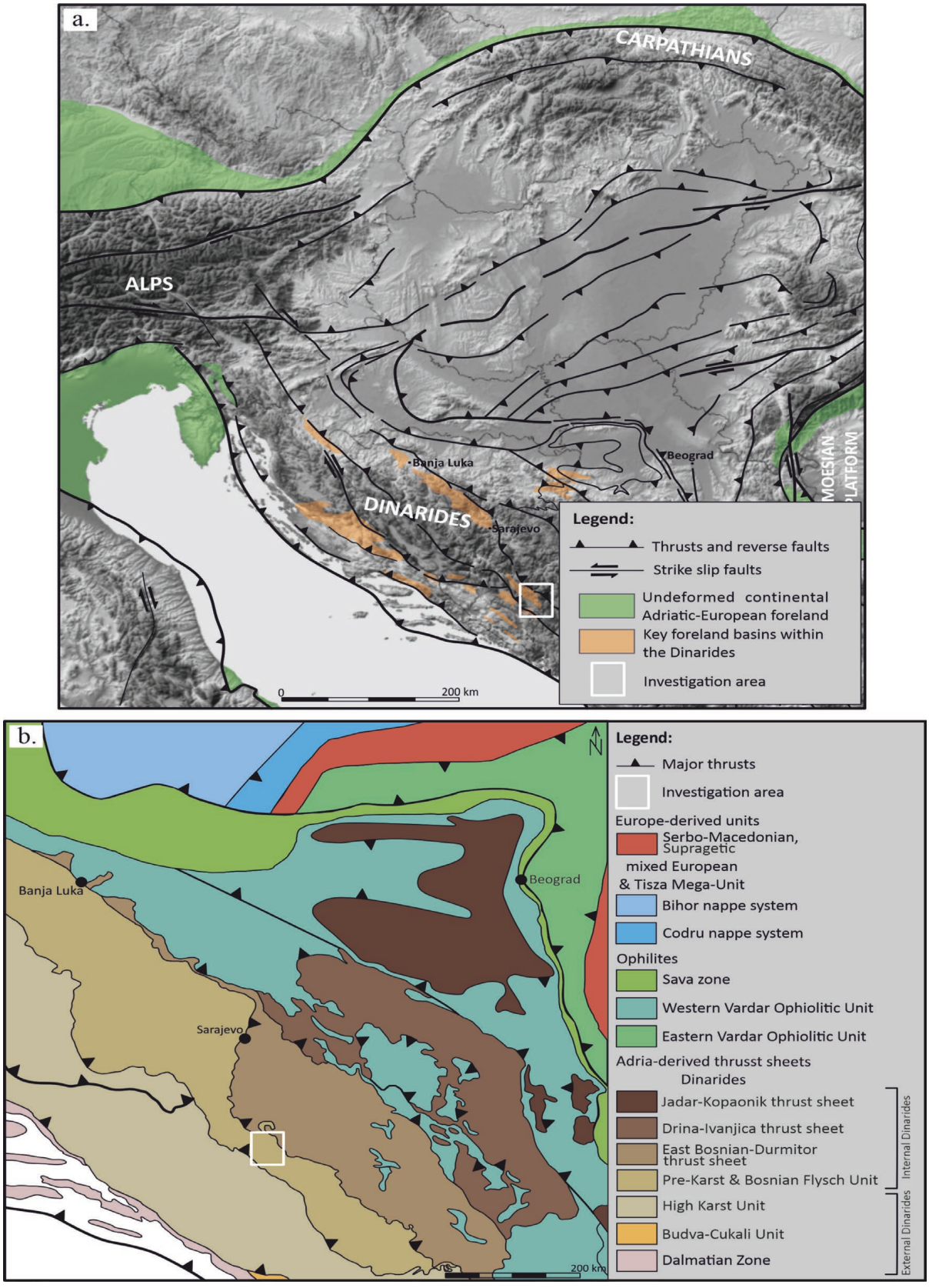

Fig. 1. (a) Shaded hypsometric map (Scilands 2015), showing the main foreland basins on the periphery of the Dinarides and Carpathians, with a focus on the main foreland basins within the Dinarides (the boundaries of the main tectonic units are shown in a simplified form according to Schmid et al. (2020); **(b)** Main tectonic units of the Dinarides (Schmid et al. 2020). The location of Gacko and its surroundings is marked on the map.

obduction, Cretaceous subduction and subsequent Late Cretaceous–Paleogene collision between the Adria (lower plate) and Europe (upper plate). During these successive tectonic stages, nappes were emplaced, representing the tectonic boundaries of the major regional units within the orogen (Stampfli & Borel 2002; Schmid et al. 2008, 2020; van Unen et al. 2019). As a result, this region represents a key segment for understanding the closure of the Neotethys in the central Mediterranean.

The Bosnian Flysch represents one of the most tectonostratigraphically complex units within the Dinaric orogen. It formed in a flexural foreland basin in front of the regional basal thrust sheet of the Eastern Bosnian-Durmitor Unit (Schmid et al. 2008; van Unen et al. 2019; Fig. 1b). The Vranduk Formation consists of Jurassic–Cretaceous turbiditic deposits, whereas the Ugar Formation comprises Upper Cretaceous–Paleogene basin fills dominated by carbonate–clastic gravity flow deposits (Mikes et al. 2008; Hrvatović 2022).

The tectonostratigraphic evolution of this basin has only been partially investigated. In its southeastern part (Fig. 2), comprehensive constraints on the age of basin-fill sequences and associated tectonic structures are still lacking. In eastern Herzegovina, in contrast to the flysch in central Bosnia (Mikes et al. 2008), the sediments of the Vranduk Formation are poorly constrained in terms of stratigraphy and spatial distribution. Their precise age, spatial extent, and relationship to the overlying Ugar Formation therefore remain unresolved.

This study aims to better constrain the age of the Vranduk and Ugar formations in eastern Herzegovina, determine the provenance of their sedimentary material, and establish the timing and tectonic mechanisms responsible for basin formation. Biostratigraphic data from microfossils and calcareous nannofossils were used to temporally calibrate the tectonostratigraphic evolution of the basin. From a tectonic perspective, the study focuses on reconstructing the kinematic evolution of the southeastern segment of the Dinarides, which is critical for understanding the broader development of the collisional system and its associated foreland basin. The post-depositional tectonic evolution of the foreland basin was inferred from structural analysis of deformation affecting the basin infill and the adjacent Neogene basin.

Tectonic framework

The Alpine–Dinaric–Mediterranean system forms part of the broad convergent plate boundary between the Eurasian and African plates (Rosenbaum et al. 2002). The Dinarides, as a segment of the Alpine–Dinaric–Mediterranean belt, represent the southeastern branch of the Alpine orogen, which continues southward into the Hellenides (Schmid et al. 2008; Handy et al. 2015). The Dinaric orogen formed during the Jurassic–Eocene convergence between Europe and Adria-derived units (Stampfli & Borel 2002; Schmid et al. 2008, 2020; Demir et al. 2019; van Unen et al. 2019).

Neotethyan rifting began in the Middle Triassic and was accompanied by magmatism and the development of the passive margin of the Adriatic plate (Dimitrijević 1997; Pamić et al. 1998, 2002; Schmid et al. 2008). Subsequently, oceanic subduction commenced during the Middle Jurassic, triggering ophiolite obduction and the formation of an ophiolitic mélange overlying the passive margin sequences of Adria. As obduction progressed, slices of oceanic lithosphere were emplaced onto the Adriatic margin (Schmid et al. 2008), followed by the thrusting of detached continental slices from the lower plate (Mikes et al. 2008). Obduction of the Western Vardar ophiolites onto the Adriatic margin began in the Late Jurassic and was accompanied by the deposition of the earliest syntectonic sediments on the flexurally deformed continental lithosphere in front of the advancing thrust front of the Adriatic plate (Mikes et al. 2008; Lužar-Oberiter et al. 2009).

Available data suggest that the siliciclastic turbiditic sequence of the Vranduk Formation was deposited from the Tithonian to the Aptian, with material sourced primarily from ophiolites (Mikes et al. 2008; Hrvatović 2022). The southern prolongation of the Vranduk Formation is represented by the Vermoshi flysch in Albania, which is of Barremian age (Marroni et al. 2009). The Vranduk Formation thus serves as a sedimentary marker of Late Jurassic–Early Cretaceous tectonic phases related to the compression within the Neotethyan oceanic domain (Marroni et al. 2009). As convergence progressed, deformation and synorogenic sedimentation migrated southwestward. The basin contracted, and sediments of the Ugar Formation, containing clasts derived from the Adriatic Carbonate Platform, were deposited (Mikes et al. 2008).

The Late Cretaceous–Paleogene was marked by the collision between continental domains of Adria and Europe (Fig. 1b). Progressive convergence led to the formation of a nappe stack and development of the Sava Suture, which delineates the boundary between these two continental domains (Pamić 2002; Schmid et al. 2008; Ustaszewski et al. 2010; Toljić et al. 2018; Demir et al. 2019).

Sedimentation patterns changed significantly during this period. In contrast to the older Vranduk Formation, which contains material derived primarily from ophiolites and continental basement units, the carbonate–clastic deposits of the Ugar Formation were sourced mainly from the margin of the Adriatic Carbonate Platform (Mikes et al. 2008). The onset of continental collision is recorded by the deposition of non-platform, deep-water syn-collisional sediments during the Upper Santonian–Maastrichtian. The peak of collisional deformation is documented by the Upper Eocene clastic turbidites and the Upper Eocene–Oligocene Promina conglomerates (Mrinjek 1993; Zupanič & Babić 2011).

The post-collisional tectonic evolution of the Dinarides was characterized by bidirectional extension, which commonly reactivated pre-existing faults and led to the development of regional detachments (Toljić et al. 2013; Andrić et al. 2017; Stojadinović et al. 2017; van Unen et al. 2019). At around 20 Ma, this extensional regime resulted in the formation of isolated intramontane basins within the Dinaric orogen, collectively

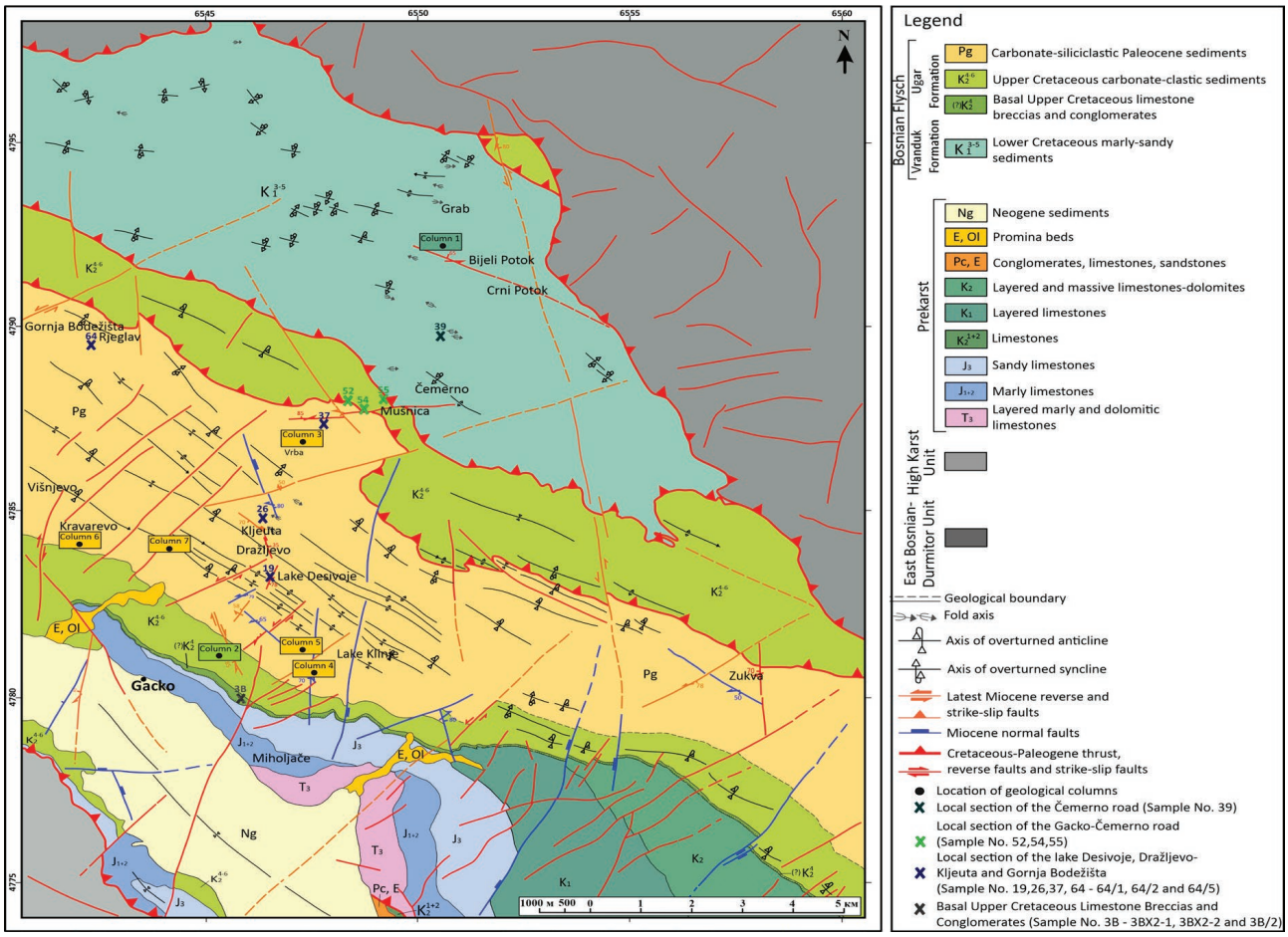

Fig. 2. Simplified geological map of the study area illustrating the distribution of the main formations. The reinterpretation is based on the 1:100,000-scale Geological Map of Yugoslavia (Mirković et al. 1980). The map displays the locations of measured geological sections and outcrops where samples for biostratigraphic analysis were collected.

referred as the Dinaride Lake System (Mandić et al. 2011; de Leeuw et al. 2010; Andrić et al. 2017).

This extensional phase was followed by renewed compression and basin inversion, which began in the Late Miocene and continues to the present day (Bada et al. 2007). These processes are driven by the indentation and counterclockwise rotation of the Adriatic plate (e.g., Márton et al. 2003; Pinter et al. 2005; Weber et al. 2010; Heidbach et al. 2016). Present-day kinematic studies indicate that the Adriatic plate indents northward, in the northwestern Dinarides, whereas in the central and southeastern segments it moves northeastward, consistent with its counterclockwise rotation (Márton et al. 2003; Pinter et al. 2005; Weber et al. 2010; Heidbach et al. 2016; Andrić et al. 2017; van Unen et al. 2019; Schmid et al. 2020).

Geological setting of eastern Herzegovina

The region of eastern Herzegovina is predominantly composed of Upper Cretaceous–Paleogene sediments of the Durmitor Flysch (Mirković et al. 1980; Fig. 2). In tectonic and paleogeographic contexts, this region has been referred to by various names, including “Flysch bosniaque & zone prékarstique” (Blanchet 1966), “Sarajevo Sigmoid” (Dimitrijević 1997), “Bosnian Flysch” (Mikes et al. 2008; Hrvatović 2022), or as “Prekarst & Bosna Flysch” (Schmid et al. 2008, 2020).

Previous studies have shown that the intensively folded sedimentary sequences commonly grouped under the term Bosnian Flysch can be subdivided into two main formations: (i) the Vranduk Formation and (ii) the Ugar Formation (Olujić 1978; Hrvatović 2022 and references therein; Ćorić & Benić 2014; Jolović et al. 2017). Deposition of the Vranduk Formation began during the Early Jurassic and became progressively younger toward the more external zones of the Dinarides during the Early Cretaceous (Schmid et al. 2008 Schmid et al. 2008).

French geologists have considered these two formations to represent a single depositional unit, resulting from continuous sedimentation spanning from the Late Jurassic to the Late Cretaceous (Rampnoux 1969; Aubouin et al. 1970; Blanchet et al. 1970). Recent stratigraphic studies indicate a Tithonian–Berriasian age for the lower part of the Vranduk Formation

(Mikes et al. 2008; Hrvatović 2022). In northern and central Bosnia, the Vranduk Formation shows a continuous stratigraphic succession ranging from the Berriasian to the Cenomanian (Cadet & Sigal 1969; Rampnoux 1969; Blanchet et al.1970; Charvet 1978). Overlying these is a carbonate–marly series assigned to the Ugar Formation (Hrvatović 2022 and references therein).

According to published geological maps and previously available biostratigraphic data (Mikes et al. 2008), the Ugar Formation has been reported as Late Albian–Maastrichtian in age. It has also been suggested to extend into the Paleogene, although this has not been clearly delineated on official geological maps (Mikes et al. 2008; Jolović et al. 2017; Hrvatović 2022).

The Vranduk and Ugar formations are separated by an angular unconformity, with the Vranduk Formation erosionally truncated at the top. This truncation is interpreted as the result of Early Cretaceous thrusting of the East Bosnian–Durmitor Unit toward the southwest (Dimitrijević 1997; Csontos et al. 2003; Hrvatović 2022).

Materials and methods

During the field investigations in eastern Herzegovina (EH), data on lithostratigraphic properties of sedimentary units were collected, and the petrographic and thin-section analyses were conducted on sediments from the Vranduk and Ugar formations. During the fieldwork and logging of local geological columns, sedimentary packages were distinguished, and representative samples were collected to better characterize the lithology. A total of fifty samples were collected for micropaleontological analysis. The micropaleontological study included identification of benthic and planktonic foraminifera, calcareous algae, calcisphaerulids, and crustacean remains, and analysis of calcareous nannofossils to constrain the age of the formations more precisely.

Smear slides for calcareous nannofossils analysis were prepared following the standard preparation technique described by Perch-Nielsen (1985). Sample preparation adhered to standardized procedures, and the samples were examined under both parallel and crossed nicols at 1000× magnification. In addition, petrographic thin sections were prepared by cutting and mounting rock billets on glass slides, grinding them to a standard thickness of 30 μm, and covering with a glass slip. These sections were examined under transmitted, plane-polarized light using a ZEISS Axio Imager 2 Pol microscope (Carl Zeiss AG, Baden-Württemberg, Germany).

Field analysis of tectonic structures and kinematic studies of faults were carried out to identify the main fault zones, determine their spatial distribution, and characterize their kinematic behaviour. Based on the collected kinematic data, a phased interpretation of the deformation history and a reconstruction of the paleostress field in which the observed structures formed were performed. The effects of deformation in the brittle domain were analysed, including fault dip angles, striations, Riedel's shears, and other parameters relevant to fault kinematics and the determination of deformation superposition. Special attention was given to recording bedding orientation and folds.

The kinematic data were analysed using the software *TectonicsFP* (Ortner et al. 2002) to perform quantitative paleostress analysis. Numerical and graphical inversion methods were applied following the approach of Angelier 1979. These methods are based on the calculation of the P, B, and T axes, where the P-axis corresponds to the maximum principal stress (σ_1), B-axis to intermediate principal stress axis (σ_2), and the T-axis to the minimum principal stress (σ_3). Paleostress modelling was performed assuming a constant angular deviation of 30° between the slip lineation and the P-axis (Angelier 1979).

Results

Vranduk Formation

The Vranduk Formation is tectonically wedged between Triassic sediments of the East Bosnian–Durmitor Unit to the northeast and the Cretaceous–Paleogene deposits of the Ugar Formation to the southwest (Fig. 2).

In eastern Herzegovina, the Vranduk Formation crops out north of Čemerno and near Grab (Fig. 2), where it is represented by a sandy–marly succession composed of three lithological packages (Fig. 3) with distinct structural and textural features. Here, the formation is predominantly composed of microconglomerates, thin-bedded marls, coarse- and fine-grained clastics, as well as alternating carbonate–sandy sediments (for details, see Supplementary Fig. S1a, b for details), with subordinate chert intercalations. The sandstones and calcarenites commonly exhibit normal grading (Supplementary Fig. S1c, d) and intervals of horizontal lamination, representing parts of Bouma sequences. Also, intraformational breccias are locally abundant.

A petrological analysis indicates that the Vranduk Formation comprises litharenites, sublitharenites, calcareous litharenites to sandy calcarenites, and poorly sorted polymictic breccias. The main detrital components include quartz, feldspar, and lithic fragments. Quartz grains exhibit variable degrees of roundness, ranging from angular to well-rounded (Fig. 4a).

In addition to quartz and feldspar, lithic fragments of mafic rocks (Fig. 4b) and serpentinized rocks (Fig. 4c) represent a significant volume of the sandstone clasts. The rock fragments also include hydrothermally altered volcanic rocks and fragments of volcanic glass. Carbonate lithoclasts containing fossil detritus (Fig. 4d) are sporadic, whereas calcite grains with distinctive twinning (Fig. 4e) and chert fragments (Fig. 4f) are rare.

The lowest unit, Package A, is characterized by a thick sequence of breccias, sandstones, marls, and interbedded layered sandstones and calcarenites, with subordinate limestones. Chert occurs as discrete intercalations. Biostratigraphic

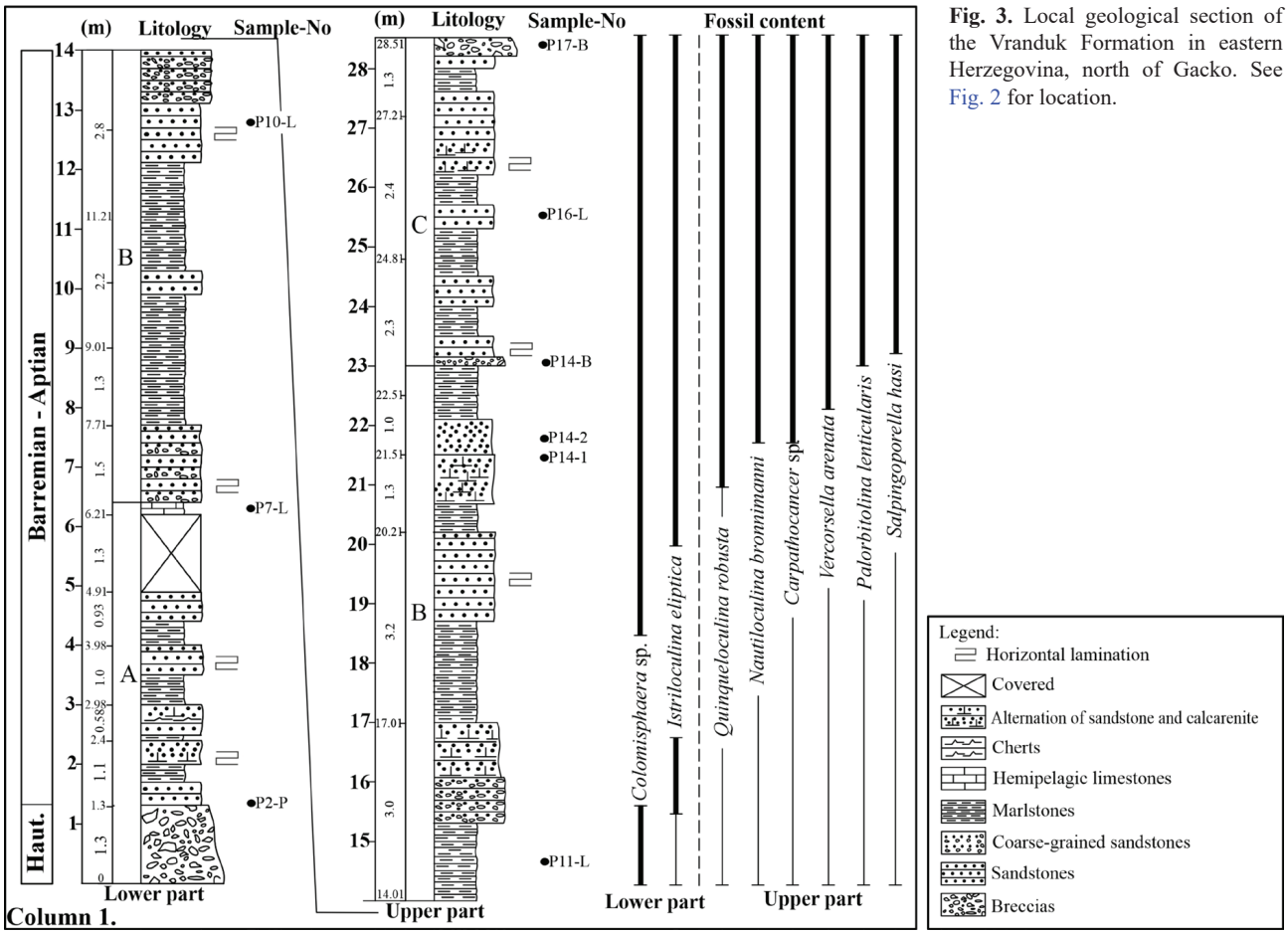

Fig. 3. Local geological section of the Vranduk Formation in eastern Herzegovina, north of Gacko. See Fig. 2 for location.

analysis of the fossil microfauna from clastic rocks in the lower part of the studied Vranduk Formation (Fig. 3; Sample No. P2-P) revealed the following assemblage: *Colomisphaera* sp. (Fig. 4h), *Istriloculina eliptica* (Iovcheva), *Protopeneroplis* sp., *?Ammobaculites* sp. (Fig. 4w) and *Glomospira* sp. (Fig. 4y). This assemblage suggests an uppermost ?Hauterivian to Barremian age. From slightly sandy, horizontally laminated hemipelagic limestones of the same succession (Fig. 3; Sample No. P7-L), small, thick-walled specimens of *Hedbergella* sp., *Globigerinelloides* sp., *Lenticulina* sp., *Pithonella* sp., and other Calcisphaerulidae (Fig. 4x$_1$) were identified. This assemblage indicates Barremian to Lower Aptian age.

Package B of the Vranduk Formation is predominantly composed of coarse-grained calcarenites, lithic sandstones, marls, sandstones, and alternating beds of calcarenites. This unit is characterized by normal and inverse grading in coarse- to medium-grained sandstone intervals, as well as by horizontal lamination in finer-grained layers. Carbonate-rich, coarse-grained litharenites from the middle stratigraphic levels of the package B (Fig. 3; Sample No. P14-1) contain calcareous lithoclasts with scleractinian corals (*"Madrepora"* sp.), Orbitolinidae, *Quinqueloculina robusta* (Neagu), *Moesiloculina* sp., *Nautiloculina* sp., and Pfenderiinae. This assemblage indicates Barremian to earliest Aptian age.

Fig. 4. Optical microscopic characteristics of representative rock samples from the Vranduk Formation (a–f) and characteristic microfossil association of the Vranduk Formation (g–y$_1$): **(a)** Well-sorted litharenites with quartz grains exhibiting varying degrees of roundness; **(b)** The ophitic texture of the diabase is formed by elongated and intercrossed plagioclase crystals; **(c)** Fragments of serpentinite with a mesh-like structure in polymictic breccia; **(d)** Orbitolinids bioclasts in polymict breccia; **(e)** Calcite with characteristic lamellar twinning; **(f)** Fragments of chert in limestone litharenites, mv – mafic volcanic lithoclast; s – serpentinite lithoclast; ch – chert; Q – quartz; pQ – polycrystalline quartz; **(g)** Clast with radiolarians; **(h)** *Colomisphaera* sp.; **(i)** *Protopeneroplis ultragranulata* (Gorbachik); **(j)** *Pseudocyclammina* cf. *lituus* (Yokohama); **(k)** *Halplophragmoides joukowsky* Charollais, Brönnimann & Zaninetti; **(l)** *Novalesia distorta* Arnaud-Vanneau; **(m)** *Redmondoides lugeoni* (Septofontaine; **(n, o)** *Quinqueloculina robusta* (Neagu); **(p)** *Textularia* sp.; **(r)** *Salpingoporella* aff. *hasi* Conrad, Radoičić & Rey and *Palorbitolina lenticularis* Blumenbach; **(s)** *Baccinella irregularis* Radoičić; **(t)** Large fragment of Requieniidae; **(u)** *"Madrepora"* sp.; **(v)** *Carpathocancer* sp.; **(w)** *Ammobaculites* sp.; **(x)** *?Orbitolina* sp.; **(y)** *Glomospira* sp.; **(z)** Nodosariidae; **(x$_1$)** Calcisphaerulidae; **(y$_1$)** Microfacies of limestone clasts in the breccia of the Vranduk Formation.

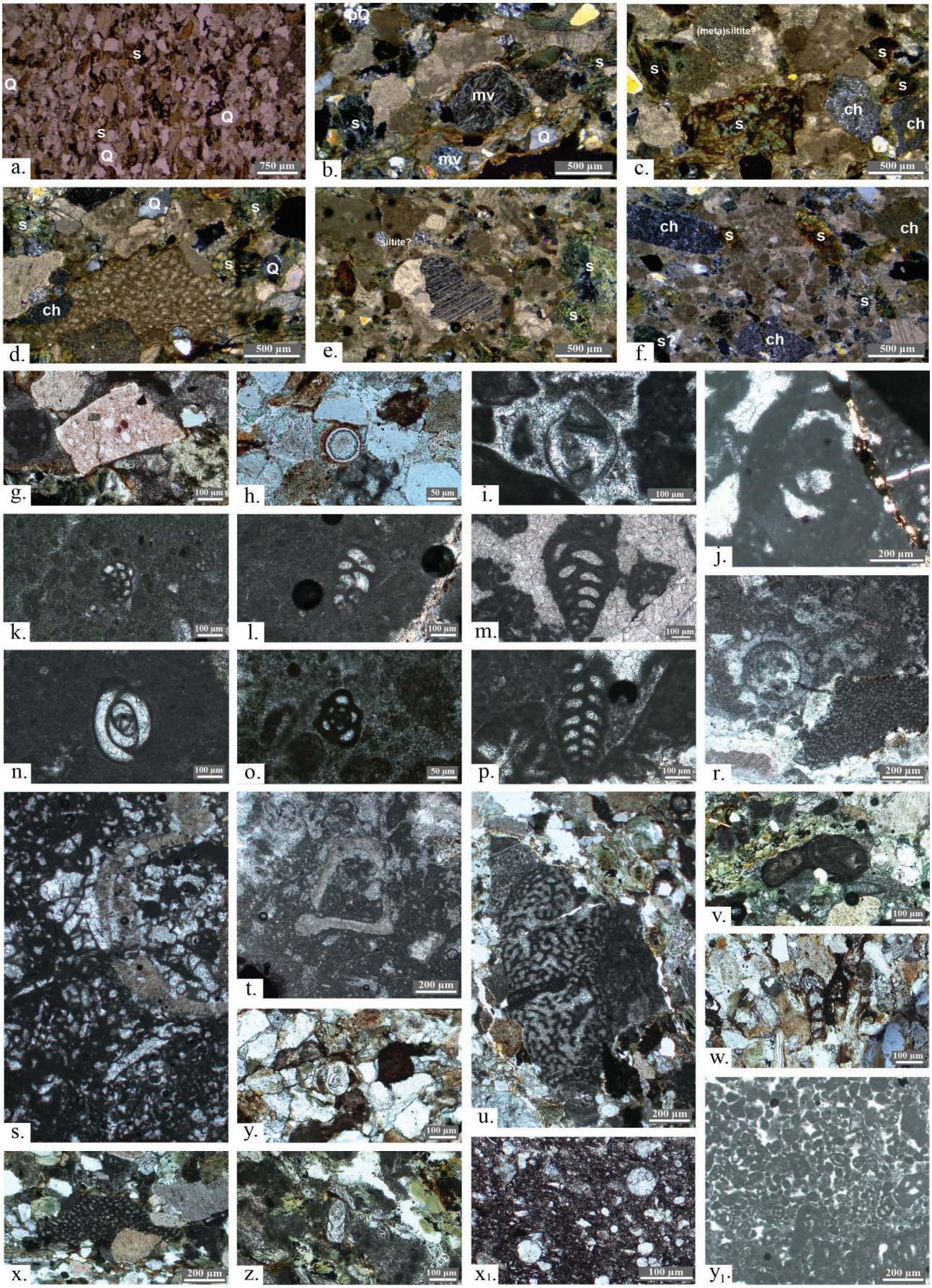
a.
Q
s
Q
s
Q
750 µm
b.
pQ
s
mv
s
Q
mv
500 µm
c.
(meta)siltite?
s
s
s
ch
s
ch
500 µm
d.
Q
s
s
s
Q
ch
500 µm
e.
siltite?
s
s
500 µm
f.
ch
s
s
ch
s
s?
ch
500 µm
g.
100 µm
h.
50 µm
i.
100 µm
j.
200 µm
k.
100 µm
l.
100 µm
m.
100 µm
n.
100 µm
o.
50 µm
p.
100 µm
r.
200 µm
s.
t.
200 µm
u.
200 µm
v.
100 µm
w.
100 µm
y.
100 µm
x.
200 µm
z.
100 µm
x1.
100 µm
y1.
200 µm

In the medium-grained calcareous litharenite from the same package (Fig. 3; Sample No. P14-2), the following taxa were identified: *Nautiloculina bronnimanni* Arnaud-Vanneau & Peybernès, *Vercorsella arenata* Arnaud-Vanneau, *Tritaxia* cf. *pyramidata* Reuss, *Haplophragmoides* sp., *Ammobaculites* sp., *Siphopfenderina* sp., *Palorbitolina* sp., *Carpathocancer* sp. (Fig. 4v), and representatives of Nodosariidae (Fig. 4z). This assemblage is also dated to Upper Barremian–Lower Aptian.

The package C consists of limestone breccias, sandstones with radiolarian clasts (Fig. 4g), and marls. The breccias (Fig. 3; Sample No. P14-B) contain the following microfossils assemblage: *Palorbitolina lenticularis* Blumenbach, *Salpingoporella* aff. *hasi* Conrad, Radoičić & Rey (Fig. 4r), *?Orbitolina* sp. (Fig. 4x), *Trochamminoides* sp., *Pseudolituonella* sp., and *Salpingoporella* sp., accompanied by macrofossil fragments of Requieniidae (Fig. 4t), and *"Madrepora"* sp. (Fig. 4u), indicating an Uppermost Barremian–Lower Aptian age. The upper-level sublitharenites (Fig. 3; Sample No. P16-L) contain rare specimens of *Hedbergella* sp. Carbonate breccias from the upper part of Package C (Fig. 3; Sample No. P17-B) include clasts derived from various stratigraphic levels (Fig. 4y1): *Quinqueloculina robusta* (Neagu) (Fig. 4n, o), *Arenobulimina* sp., *Istriloculina* sp., *Pseudocylamina* cf. *lituus* (Yokohama) (Fig. 4j), *Haplophragmoides* cf. *jaukowskyi* Charrolais (Fig. 4k), *Novalesia distorta* Arnaud-Vanneau (Fig. 4l), *Sabaudia minuta* (Hofker), (Fig. 4p), *Protopeneroplis striata* Weynschenk (Fig. 4i), *Istriloculina* cf. *eliptica* (Iovcheva) (see Supplementary Table S1 for accompanying taxa). Parts of the thin section are occupied by microbial *Bacinella* structure (Fig. 4s), indicating environmental changes related to locally developed anoxic conditions within the basin (Conrad & Clavel 2008). The clasts are dated to ?uppermost Hauterivian–Barremian. However, the breccia itself may be either coeval or of Aptian age.

Calcareous nannofossil analysis was performed on samples collected from outcrops north of Čemerno (Fig. 2; Sample No. 39). The identified taxa include *Watznaueria biporta* Bukry, 1969 (Fig. 5-4), *Braarudosphaera africana* Stradner, 1961 (Fig. 5-25), and *Braarudosphaera hockwoldensis* Black, 1973 (Fig. 5-30), which collectively indicate an Albian age.

Ugar Formation

The Ugar Formation in eastern Herzegovina extends northward from Gacko towards Čemerno (Fig. 2). Tectonically, it is situated between the limestones of the High Karst Zone to the southwest and the clastic deposits of the Vranduk Formation to the northeast (Fig. 2). In the investigated area, three members can be distinguished within the Ugar Formation: (1) basal limestone breccias and conglomerates, (2) Upper Cretaceous carbonate–clastic sediments, and (3) Paleocene carbonate–siliciclastic sediments.

Basal Upper Cretaceous limestone breccias and conglomerates

Sedimentation of the Upper Cretaceous succession begins with a series of basal limestone breccias and conglomerates of variable thickness (Supplementary Fig. S1e). The breccias and conglomerates are composed of angular to poorly rounded clasts cemented by carbonate. Graded bedding and turbidite flow structure are absent, indicating that this succession lacks turbiditic characteristics. Depending on the type of allochems and the binding material, limestone fragments within breccias and conglomerates are clasified as biomicrudites, biosparites, biomicrites, and micrites.

Planktonic foraminifera from the studied basal limestone breccias and conglomerates were identified in biomicrites (Fig. 2; Sample No. 3BX2-1 and 3BX2-2) and include *Marginotruncana coronata* (Bolli), *Dicarinella* cf. *canaliculata* (Reuss), *Dicarinella concavata* (Brotzen) (Fig. 6b), *Whiteinella* cf. *paradubia* (Sigal), *Marginotruncana pseudolinneiana* Pessagno (Fig. 6c), *Marginotruncana* cf. *marginata* (Reuss), *Pithonella sphaerica* (Kaufmann), *Planoheterohelix reussi* (Cushman), along with *Cuneolina* sp. and other benthic foraminifers. This assemblage indicates a possible age range from the latest Turonian–Coniacian to Early Santonian. In biomicrites from Sample No. 3B/2, the following foraminifers were identified: *Dicarinella concavata* (Brotzen), *Whiteinella archaeocretacea* Pessagno (Fig. 6a), *Pithonella sphaerica* (Kaufmann) (Fig. 6d). This fossil association suggests an age from the Coniacian to the earliest Santonian.

Fig. 5. Nannoplancton identified in samples taken northern from Gacko: 1. *Watznaueria leesiae* Young 2023; 2. *Watznaueria britannica* (Stradner 1963); 3. *Watznaueria fossacincta* (Black 1971); 4. *Watznaueria biporta* Bukry, 1969; 5. *Watznaueria barnesiae* (Black in Black & Barnes, 1959) Perch-Nielsen 1968; 6. *Semihololithus priscus* Perch-Nielsen 1973; 7. *Chiasmolithus danicus* (Brotzen 1959) Hay & Mohler 1967; 8. *Chiasmolithus danicus* (Brotzen 1959) Hay & Mohler 1967; 9. *Toweius* sp.; 10. *Coccolithus pelagicus* (Wallich 1877), Schiller 1930; 11. *Prinsius martinii* (Perch-Nielsen 1969) Haq 1971; 12. *Sphenolithus moriformis* (Brönnimann & Stradner 1960), Bramlette & Wilcoxon 1967; 13. *Sphenolithus* cf. *moriformis* (Brönnimann & Stradner 1960), Bramlette & Wilcoxon 1967; 14. *Ericsonia media* Bown 2016; 15. *Ericsonia subpertusa* Hay & Mohler 1967; 16. *Prinsius bisulcus* (Stradner 1963) Hay & Mohler 1967; 17. *Cruciplacolithus tenuis* (Stradner 1961) Hay & Mohler, Hay et al. 1967; 18. *Cruciplacolithus asymmetricus* van Heck & Prins 1987; 19. *Calcareous dinoflagellate*; 20a. *Micula staurophora* (Gardet 1955) Stradner 1963; 20b. *Cyclagelosphaera reinhardtii* (Perch-Nielsen 1968) Romein 1977; 21. *Ellipsolithusdistichus* (Bramlette & Sullivan 1961), Sullivan 1964; 22. *Lithoptychius* sp.; 23. *Fasciculithus billii* Perch-Neielsen 1971; 24. *Uniplanrius gothicus* (Deflandre 1959), Hattner & Wise, in Wind & Wise 1983; 25. *Braarudosphaera africana* Stradner 1961; 26. *Braarudosphera bigelowii* (Gran & Braarud 1935), Deflandre 1947; 27. *Fasciculithus involutus* Bramlette & Sullivan 1961; 28. *Neochiastozygus* cf. *concinnus* (Martini 1961); 29. *Tectulithus pileatus* (Bukry 1973), Miniati et al. 2021; 30. *Braarudosphaera hockwoldensis* Black 1973; 31. *Microrhabdulus decoratus* Deflandre 1959; 32. *Arkhangelskiella cymbiformis* Vekshina 1959; 33. *Eiffellithus eximius* (Stover 1966), Perch-Nielsen 1968; 34. *Placozygus fibuliformis* (Reinhardt 1964) Hoffmann 1970; 35. *Lucianorhabdus* sp.

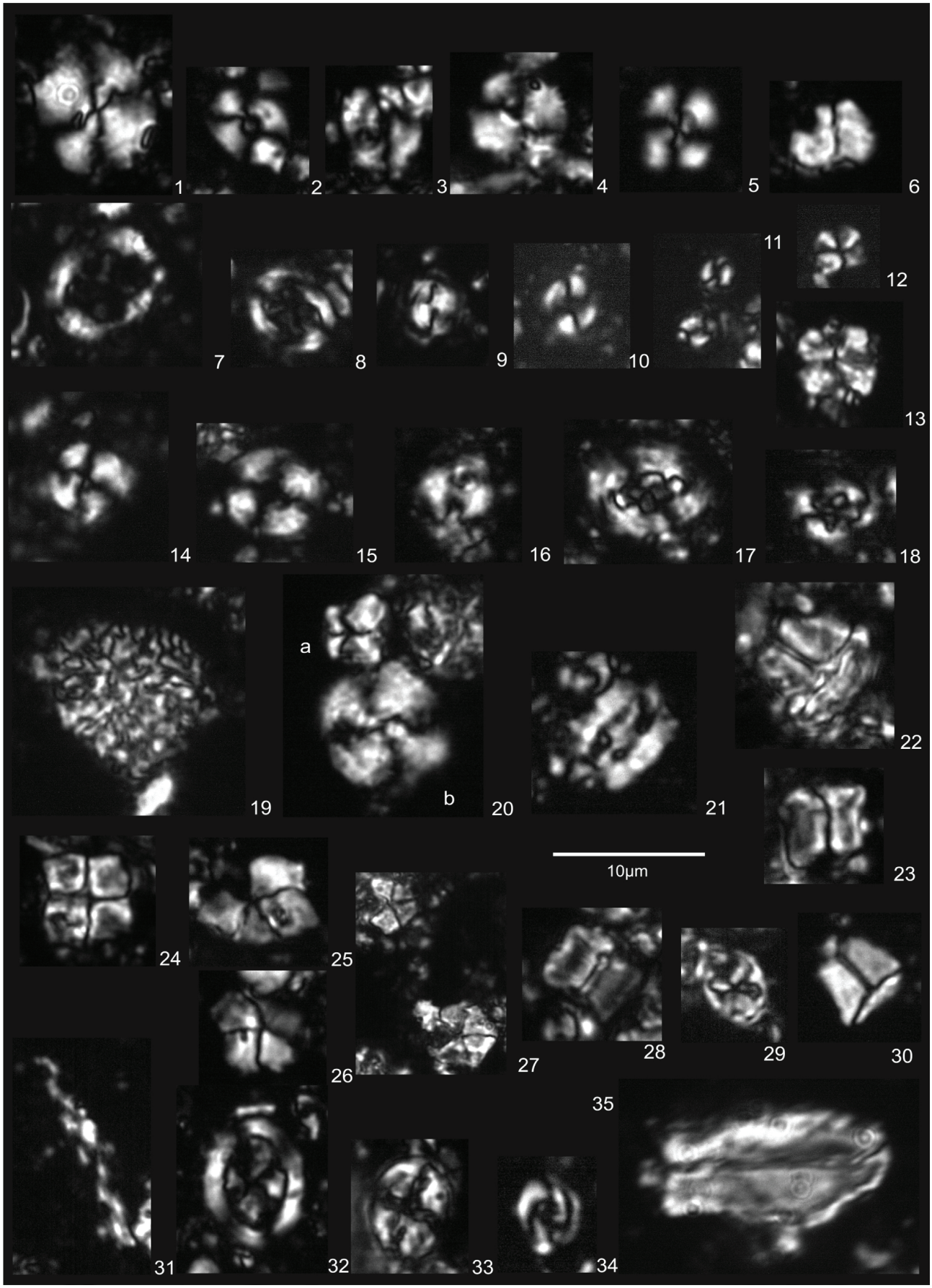
1
2
3
4
5
6
7
8
9
10
11
12
13
14
15
16
17
18
a
b
19
20
21
22
23
10µm
24
25
26
27
28
29
30
31
32
33
34
35

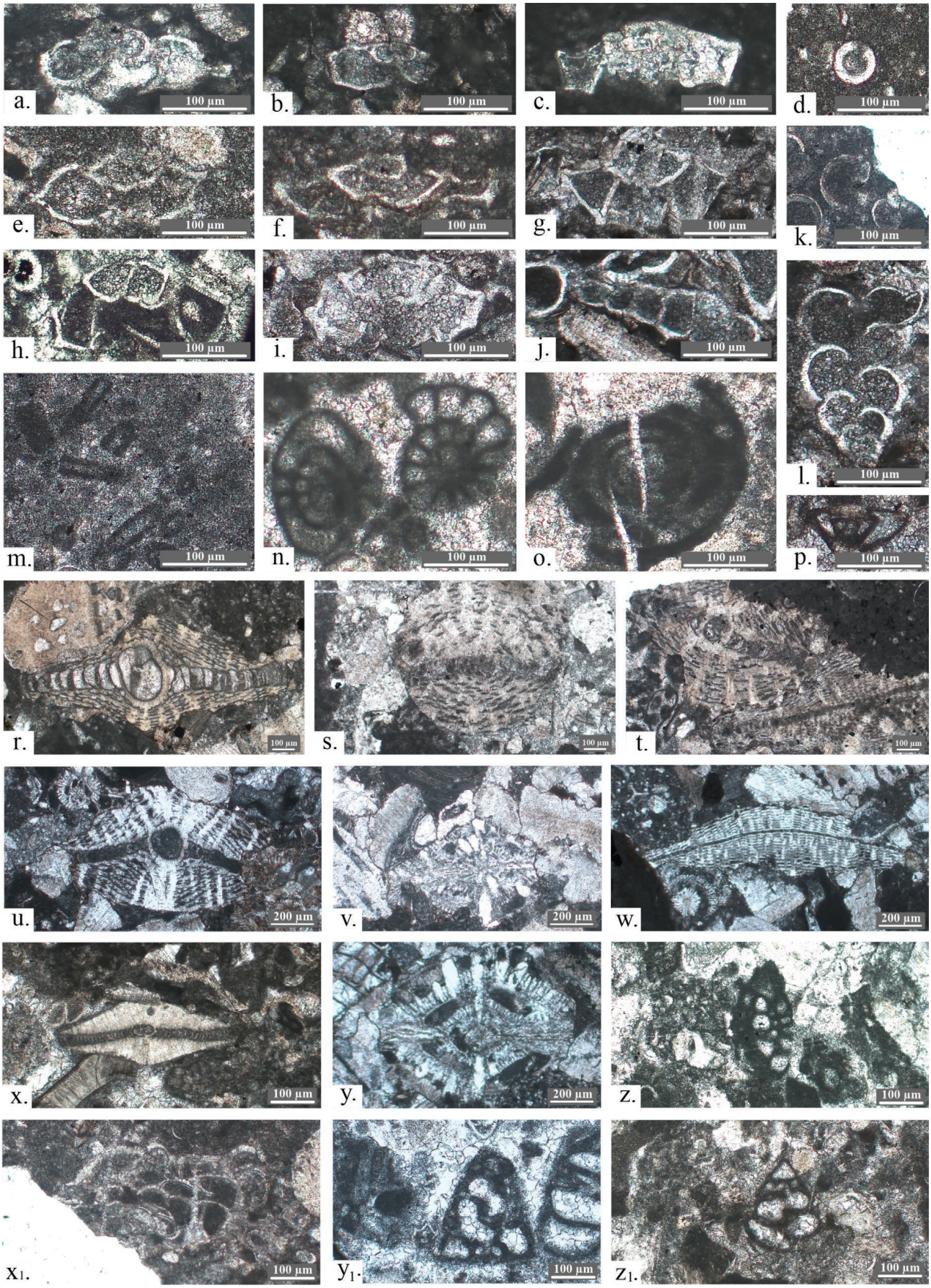
a.
100 µm
b.
100 µm
c.
100 µm
d.
100 µm
e.
100 µm
f.
100 µm
g.
100 µm
k.
100 µm
h.
100 µm
i.
100 µm
j.
100 µm
l.
100 µm
m.
100 µm
n.
100 µm
o.
100 µm
p.
100 µm
r.
100 µm
s.
100 µm
t.
100 µm
u.
200 µm
v.
200 µm
w.
200 µm
x.
100 µm
y.
200 µm
z.
100 µm
x1.
100 µm
y1.
100 µm
z1.
100 µm

Fig. 6. Upper Cretaceous microfossil association of the Ugar Formation, north of Gacko: **(a)** *Whiteinella archaeocretacea* Pessagno; **(b)** *Dicarinella concavata* (Brotzen); **(c)** *Marginotruncana pseudolinneiana* Pessagno; **(d)** *Pithonella sphaerica* (Kaufmann); **(e)** *Marginotruncana schneegansi* (Sigal); **(f)** *Margintoruncana* cf. *tarfayaensis* (Lehmann); **(g)** *Globotruncanita stuartiformis* (Dalbiez); **(h)** *Contusotruncana fornicata* Plummer; **(i)** *Globotruncana arca* (Cushman); **(j)** *Planoglobulina acervulinoides* (Egger); **(k)** *Bonetocardiella conoidea* (Bonet); **(l)** *Planoheterohelix globulosa* (Ehrenberg); **(m)** *Decastronema kotori* (Radoičić); **(n)** *Moncharmontia apenninica* (De Castro); **(o)** *Vidalina hispanica* Schlumberger; **(p)** *Cibicidoides* sp.; **(r)** *Orbitoides media* (d'Archiac); **(s)** *Orbitoides* cf. *media* (d'Archiac); **(t)** *Orbitoides apiculata* Schlumberger and *Lepidorbites socialis* (Leymerie); **(u)** *Orbitoides apiculata* Schlumberger with *Siderolites calcitrapoides*; **(v)** *Siderolites calcitrapoides* Lamarck & Coraliinaceae; **(w)** *Lepidorbitoides* cf. *socialis* (Leymerie); **(x)** *Hellenocyclina beotica* Reichel; **(y)** *Siderolites calcitrapoides* Lamarck; **(z)** *Fleuriana adriatica* De Castro, Drobne & Gušić; **(x_1)** *Planorbulina? cretae* (Marsson); **(y_1, z_1)** *Valvulina triangluaris* (d'Orbigny).

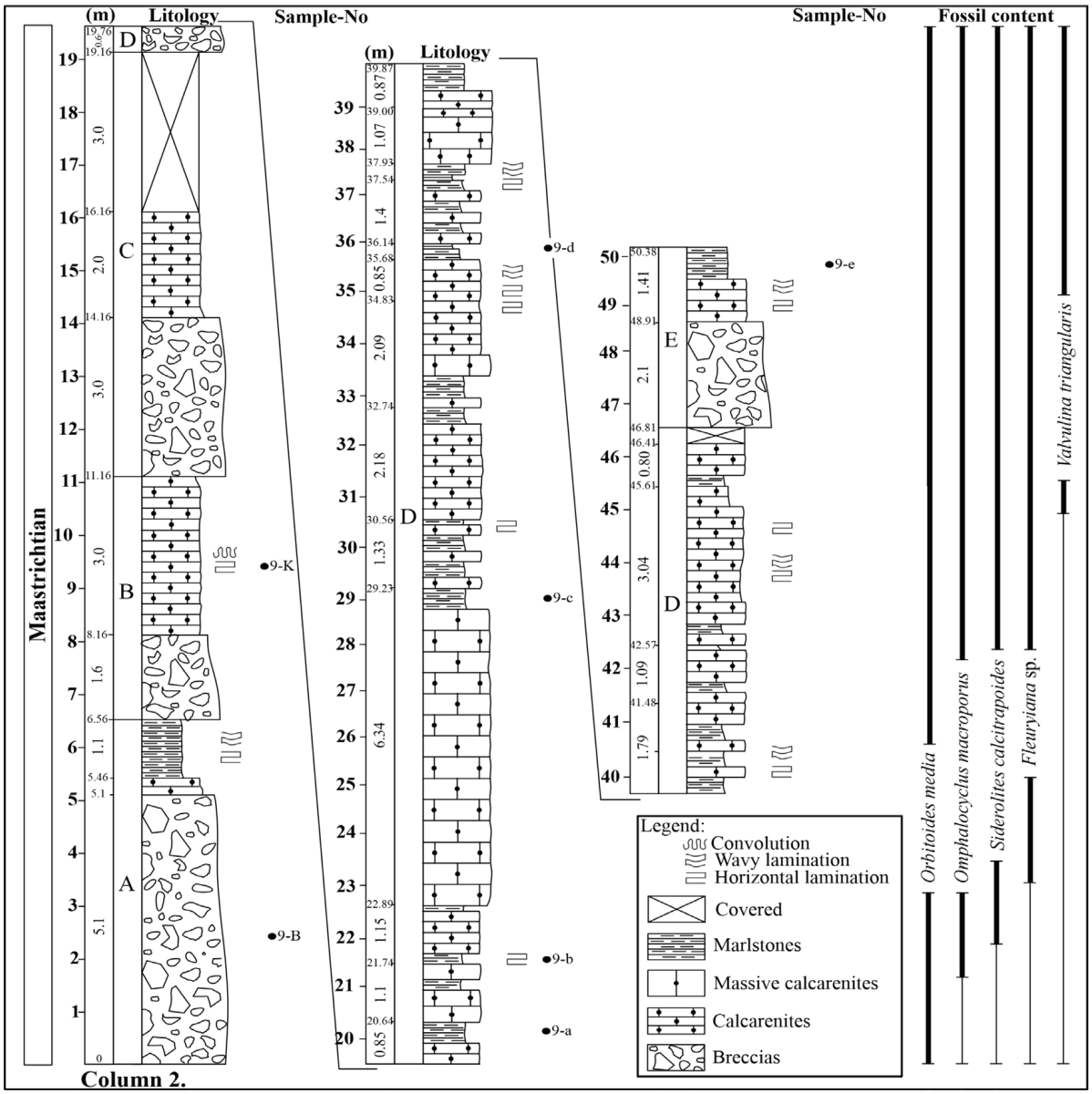

Fig. 7. Local geological section of Upper Cretaceous carbonate deposits north of Gacko. See Fig. 2 for location.

Upper Cretaceous carbonate–clastic sediments

Upper Cretaceous carbonate–clastic succession comprises limestones, marly limestones, marls with interbeds of calcarenites, and siliceous mudstones (Fig. 7). These sediments transgressively overlie the basal breccias and conglomerates. A characteristic feature of the Upper Cretaceous carbonate–clastic series is the presence of packages of intraformational limestone breccias (Supplementary Fig. S1f). Limestones display intervals of normal grading (Supplementary Fig. S1g),

most commonly starting with a lower interval of horizontal lamination (Tb), followed by convolute lamination (Tc), and ending with an upper interval of horizontal lamination (Td, Supplementary Fig. S1h).

Petrographic analysis indicates that the studied carbonates consist of biomicrudites, biosparites, micrites, biomicrites, biopelmicrites, and biointramicrites. Allochthonous components are predominantly of biogenic origin.

Biostratigraphic analyses were conducted at several spatially separate localities and across superpositionally different levels of the studied limestone succession. The observed sections exhibits an rhythmic alternation of breccias and calcarenites, often associated with finer-grained marly layers.

Package A consists mainly of breccias, calcarenites, and marls. In different clasts of breccias (Fig. 7; Sample No. 9-B), the following foraminifera were identified: *Orbitoides media* (d'Archiac) (Fig. 6r), *Omphalocyclus macroporus* (Lamarck), *Siderolites calcitrapoides* Lamarck, *Fleuryana* sp.; *Pseudocyclammina sphaeroidea* Gendrot, *Vidalina hispanica* Schlumberger; *Marginotruncana schneegansi* (Sigal) (Fig. 6e), *Marginotruncana* cf. *tarfayaensis* (Lehmann) (Fig. 6f), *Globotruncanita stuartiformis* (Dalbiez), accompanied with *Rotorbinela* sp.*; Neodubrovnikella* sp., *Cornuspira* sp., etc. (see Supplementary Table S2 for accompanying taxa). The oldest clast in this breccia is of possible Cenomanian age, while the youngest clasts correspond to the Maastrichtian. Therefore, the breccia itself is interpreted to be of late Maastrichtian age.

Package B, consisting of breccias and calcarenites, contains intrabasinally redeposited fragments of Upper Cretaceous and Maastrichtian microfauna within shelf limestone clasts (Fig. 7; Sample No. 9-K): *Vidalina hispanica* Schlumberger (Fig. 6o), *Pararotalia minimalis* Hofker, *Marginotruncana* sp., *Siderolites calcitrapoides* Lamarck, *Valvulina triangularis* d'Orbigny, *Rhapydionina* sp. Within the hemipelagic sediment part (Fig. 7; Sample No. 9K), the following planktonic foraminifera were observed: *Globotruncanita stuartiformis* (Dalbiez), *Contusotruncana* cf. *fornicata* (Plummer), *Planoheterohelix globulosa* (Ehrenberg), *Dicarinella* sp., *Reusella* cf. *szajnochae* (Grzibowski).

In package C, which is mainly composed of breccias and calcarenites, no fossil fauna was identified. Package D, consisting of breccias, calcarenites, and marls, yielded calcareous nannofossils indicating Maastrichtian age. Identified taxa include *Watznaueria leesiae* Young, 2023 (Fig. 5-1), *Watznaueria britannica* (Stradner, 1963), Reinhardt, 1964 (Fig. 5-2), *Watznaueria fossacincta* (Black 1971), Bown in Bown & Cooper, 1989 (Fig. 5-3), *Watznaueria barnesiae* (Black in Black & Barnes 1959), Perch-Nielsen, 1968 (Fig. 5-6), *Semihololithus priscus* Perch-Nielsen 1973 (Fig. 5-7), *Micula staurophora* (Gardet, 1955), Stradner, 1963 (Fig. 5-20a), *Cyclagelosphaera reinhardtii* (Perch-Nielsen, 1968) Romein, 1977 (Fig. 5-20b), *Uniplanarius gothicus* (Deflandre, 1959), Hattner & Wise, in Wind & Wise 1983 (Fig. 5-24), *Microrhabdulus decoratus* Deflandre, 1959 (Fig. 5-31), *Arkhangelskiella cymbiformis* Vekshina, 1959 (Fig. 5-32), *Eiffellithus eximius* (Stover, 1966), Perch-Nielsen, 1968 (Fig. 5-33), *Placozygus fibuliformis* (Reinhardt, 1964), Hoffmann 1970 (Fig. 5-34).

In package E, composed of breccias, calcarenites, and marls, also yielded calcareous nannofossils indicating Maastrichtian age.

Upper Cretaceous carbonate–clastic turbidites were also identified along the Gacko–Čemerno road. Biostratigraphic data indicate that these turbidites belong to the Maastrichtian sequence and have been displaced along an internal thrust, having been exhumed from the deeper part of the flysch succession (Fig. 2; locations marked as 52, 54, and 55).

In sandy-calcareous turbiditic sediments west of the Mušnica River (Fig. 2; Sample No. 52), transported benthic and planktonic organisms include *Moncharmontia apenninica* (De Castro) (Fig. 6n), *Globotruncanita* sp., *Contusotruncana* sp., *Pararotalia* cf. *tuberculifera* Reuss. These microfossils indicate an Upper Santonian–Campanian age for this assemblage.

In biomicrites from the Mušnica River area (Fig. 2; Sample No. 54), characteristic planktonic foraminifera comprise *Globotruncanita stuartiformis* (Dalbiez) (Fig. 6g), *Globotruncana arca* (Cushman) (Fig. 6i), *Planoheterohelix globulosa* (Ehrenberg) (Fig. 6l), *Contusotruncana fornicata* (Plummer), *Radotruncana* cf. *subspinosa* (Pessagno), *Planoglobulina acervulinoides* (Egger) (Fig. 6j) and *Cibicidoides succedens* (Brotzen) (Fig. 6p), indicating Upper Campanian–Maastrichtian age.

North of the Mušnica River in biointramicrites (Fig. 2; Sample No. 55), planktonic and benthic foraminifera of Campanian age were identified, including *Globotruncana arca* (Cushman), *Globotruncana linneiana* (d'Orbigny), *Rugoglobigerina rugosa* (Plummer), *Planoglobulina acervulinoides* (Egger), *Minouxia* cf. *lobata* Gendrot.

Paleocene carbonate–siliciclastic sediments

The widest NW–SE-trending unit in the Gacko area is part of a heterogeneous carbonate–siliciclastic Paleocene series, composed of limestone breccias, sandy limestones, marly limestones, calcarenites, and marls (Fig. 2). Intervals with convolute bedding and parallel lamination, characteristic of Bouma sequence structures, are well developed (Supplementary Fig. S2a, b). The sandstones occur in relatively thin layers, and the turbidites themselves are of carbonate–siliciclastic composition (Supplementary Fig. S2c). Sole marks, such as groove casts, are preserved on the lower bedding surfaces (Supplementary Fig. S2d), while current marks (Supplementary Fig. S2e) and flute casts (Supplementary Fig. S2f) are present on the upper bedding surfaces.

The petrographic characteristics of the Paleocene limestone breccias, sandy limestones, marly limestones, calcarenites, and marls correspond to carbonate microfacies including biomicrites, biointramicrudites, biomicrosparites, biosparites, and biointrasparrudites. The allochems of these rocks are mostly bioclasts, skeletal remains of organisms, or intraclasts,

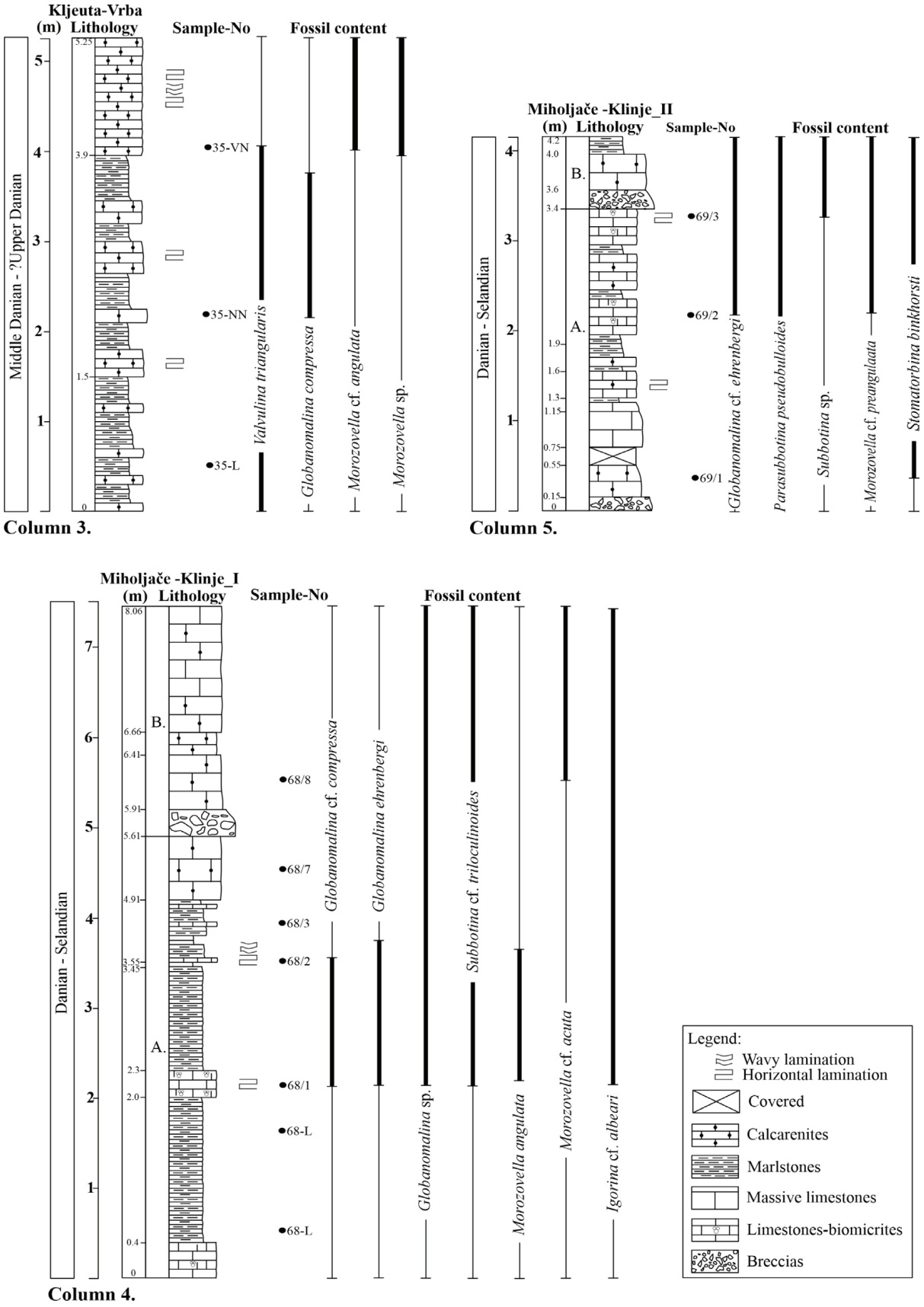

Fig. 8. Geological sections of the carbonate–clastic Paleogene succession of the Ugar Formation: **(a)** Kljeuta–Vrba profile; **(b)** Miholjače–Klinje (I) profile; **(c)** Klinje–Miholjače (II) profile.

whereas the orthochem consists of micrite or microsparite. The intraclasts are complex in type and may include fragments of consolidated biomicritic limestones. Some bioclasts display rounding and are surrounded by thick micritic coatings (cortoids). Sandy and silt-sized fractions are commonly present in the rock matrix, indicating deposition under moderate- to high-energy, open marine conditions. The sandy component comprises quartz, plagioclase, and muscovite.

The Paleocene deposits were examined in several profiles: Kljeuta–Vrba (Fig. 2; location 3), Miholjače–Klinje I (Fig. 2; location 4), Miholjače–Klinje II (Fig. 2; location 5), Kravarevo and Višnjevo (Fig. 2; location marked as 6), and Bahori–Gornja Bodežišta (Fig. 2; location 7).

At the Kljeuta–Vrba profile, the lower levels of the carbonate–clastic series are represented by marly–carbonate sediments. Nannoplankton species identified at this location (Fig. 8; location 3, Sample No. 35-L) include *Cruciplacolithus asymmetricus* (van Heck & Prins 1987) (Fig. 5-18), which indicates a Danian age for the sandy–carbonate sediments (Fig. 8; Sample No. 35-L). The middle levels of the studied sandy–limestone series (Fig. 8, location 3; Sample No. 35-NN) contain *Globanomalina* cf. *compressa* (Plummer), *Morozovella* sp., *Parasubbotina* sp., and other globigerinoid foraminifers. This fossil assemblage suggests a middle–late Danian age (Fig. 8; Sample No. 35-NN). The upper levels of the Paleocene series are carbonate-rich, represented by biomicrosparites (Fig. 8; location 3, Sample No. 35-VN) containing numerous benthic foraminifera and less frequent planktonic foraminifera, including *Cibicidoies succedens* (Brotzen), *Stomatorbina binkhorsti* (Reuss), *Valvulina triangularis* d'Orbigny (Fig. 6z$_1$), *Valvulineria bacetai* Serra-Kieol, Vicedo, Baceta, Bernaola & Robador (Fig. 9w, x, y), *Morozovella* cf. *angulata* (White), and *Planorbulinella* sp. indicating a probable late Danian age (Sample No. 35-VN).

At the Miholjače–Klinje (I) profile, two packages have been distinguished. Package A consists of fossil-rich limestones, cyclically interbedded marls, and calcarenites. In the fine-grained marls (Fig. 8; location 4, Sample No. 68-L), calcareous nannoplankton identified include *Chiasmolithus danicus* (Brotzen, 1959), Hay & Mohler 1967 (Fig. 5-8), *Sphenolithus moriformis* (Brönnimann & Stradner 1960), Bramlette & Wilcoxon,1967 (Fig. 5-12), *Ericsonia media* Bown, 2016 (Fig. 5-14), *Cruciplacolithus tenuis* (Stradner, 1961), Hay & Mohler in Hay et al., 1967 (Fig. 5-17), calcareous dinoflagellates (Fig. 5-19). This nannofossil assemblage indicates a Selandian age.

In the biomicrites, planktonic foraminifera were identified (Fig. 8; location 4, Samples No. 68/1, 68/2, and 68/3): *Globanomalina compressa* (Plummer) (Fig. 9b), *Globanomalina ehrenbergi* (Bolli) (Fig. 9c), *Globanomalina pseudomenardii* (Bolli) (Fig. 9d), *Subbotina* cf. *triloculinoides* (Plummer), *Morozovella angulata* (White), *Morozovella* cf. *aequa* (Fig. 9l), *Igorina* cf. *albeari* (Cushman & Bermudez), *"Rotalina" cayeuxi* (De Lapparent). Weakly arenaceous biomicrites of these levels contain *Morozovella* sp. and ?*Subbotina* sp. foraminifers. This fossil assemblage suggests an latest Danian? to early Selandian age. In the massive calcarenites of the studied succession (Fig. 8; location 4, Sample No. 68/7), rare *Subbotina* sp., *Parasubbotina* sp. were identified, indicating a late Danian to earliest Selandian age.

Package B is composed of intraformational limestone breccias and massive calcarenites. In the calcarenites (Fig. 8; location 4, Sample No. 68/8), *Morozovella* cf. *acuta* (Toulmin), and other truncorotaliids were identified.

At the Miholjače–Klinje (II) profile, two packages can also be distinguished. Package A is predominantly composed of breccias, biocalcarenites, limestones, and marls. The medium- to coarse-grained biocalcarenites (Fig. 8; location 5, Sample No. 69/1) contain reworked Maastrichtian microfauna: *Hellenocyclina beotica* Reichel (Fig. 6x), *Siderolites calcitrapoides* Lamarck, *Omphalocyclus macroporus* (Lamarck), *Nummofallotia cretacea* (Schlumberger), Corallinaceae (Fig. 9z$_1$), as well as Paleocene *Planorbulina? antiqua* Manguin (Fig. 9p), *Stomatorbina binkhorsti* (Reuss) (Fig. 9r, s), *Idalina sinjarica* Grimsdale (Fig. 10z), *Idalina* sp. (Fig. 9x$_1$). Foraminifera of Danian age were identified in biocalcarenites (Fig. 8; location 5, Sample No. 69/2): *Parasubbotina pseudobulloides* (Plummer), *Planorbulinella* cf. *dordoniensis* Hoffker, *Sistanites* sp. In the biomicrites (Fig. 8; location 5, Sample No. 69/2 and Sample No 69/3), the assemblage comprising *Globanomalina* cf. *ehrenbergi* (Bolli), *Subbotina* sp., *Morozovella* cf. *praeangulata* (Blow) indicates a late Danian to earliest Selandian age (for accompanying taxa, see Supplementary Table S2). Package B consists of breccias, massive calcarenites, and marls lacking diagnostic fossil fauna.

At the Kravarevo–Višnjevo profile, in the lower part of the studied succession (Fig. 10; location 6, Sample No. 62/1), the following species were identified in biomicrites: *Morozovella angulata* (White) (Fig. 9i), *Morozovella* cf. *velascoensis* (Cushman), *Morozovella occlusa* (Loeblich & Tappan) (Fig. 9j), *Globanomalina pseudomenardii* (Bolli), *Globanomalina* cf. *champani* (Parr) (Fig. 9e), and *Subbotina* cf. *triloculinoides* (Plummer). In biomicrites (Fig. 10, location 6, Sample No. 62/2), the following species were determined: *Morozovella aequa* (Cushman & Renz) (Fig. 9k), *Morozovella* ex gr. *velascoensis* (Cushman), *Morozovella angulata* (White), *Morozovella* cf. *pasionensis* (Bermudez), and other planktonic foraminifera (Fig. 9m). This fossil assemblage indicates an upper Selandian to lower Thanetian age.

The middle level of the studied clastic–carbonate succession (Fig. 10, location 6, Sample No. 62/4) contains the following assemblage: *Morozovella aequa* (Cushman & Renz), *Morozovella* cf. *pasionensis* (Bermudez), *Subbotina triloculinoides* (Plummer) (Fig. 9f, g, h), *Valvulina triangularis* d'Orbigny (Fig. 6y$_1$), and *Stomatorbina* sp. (Fig. 9t). This assemblage suggests a Selandian–Thanetian age. The upper levels of the studied succession (Fig. 10; location 6, Sample No. 62/5) contain reworked Cretaceous foraminifera, including *Pararotalia* cf. *minimalis* Hofker, *Sulcoperculina* sp., *Rotorbinella lepina* Consorti, Frijia & Caus, cyanobacterium *Decastronema kotori* (Radoičić), rare *Cymopolia* sp., Dasycladaceae.

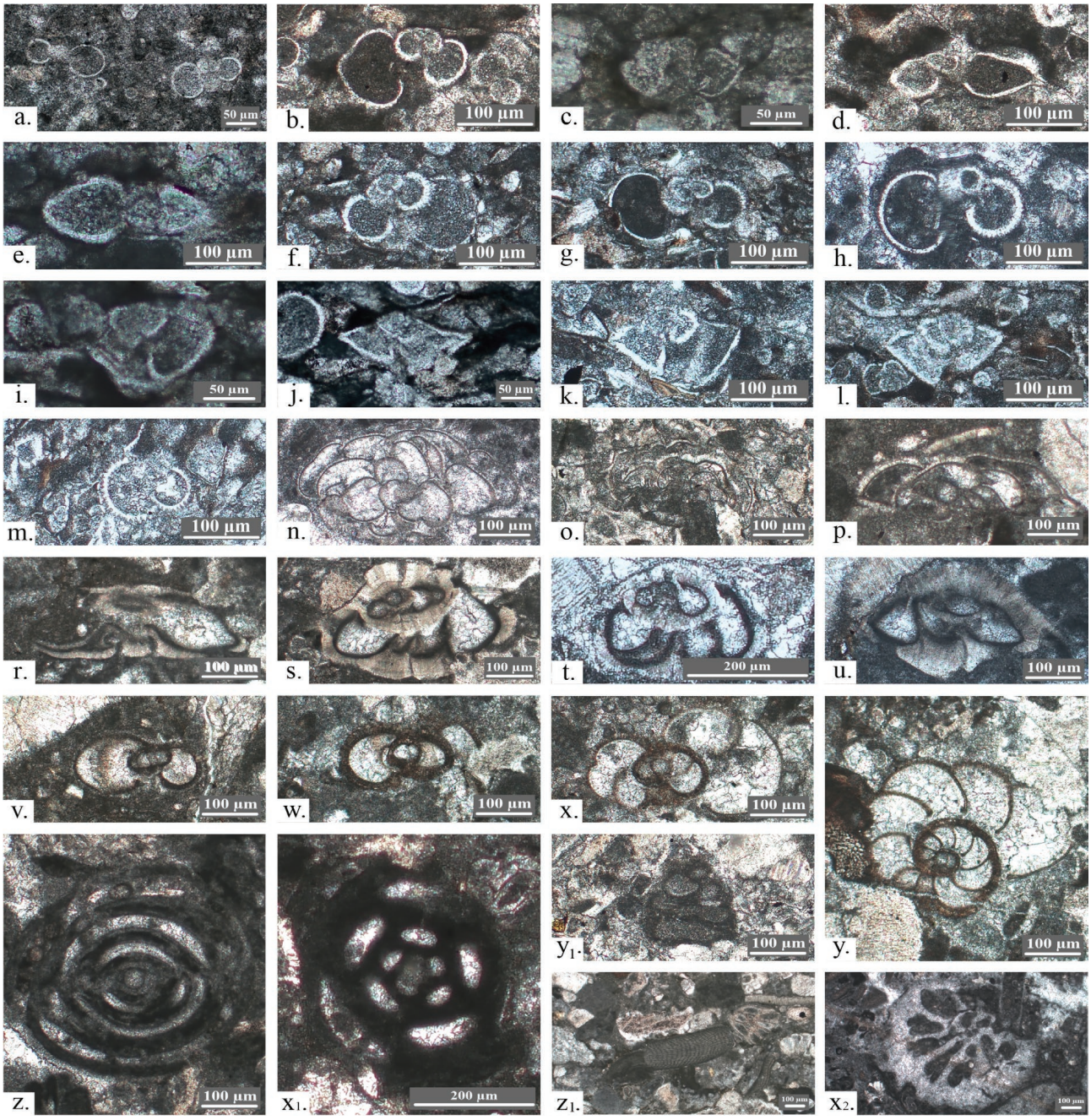

Fig. 9. Characteristic Paleogene microfossil association of the Ugar Formation: **(a)** *Globanomalina* cf. *archeocompressa* (Blow); **(b)** *Globanomalina compressa* (Plummer); **(c)** *Globanomalina ehrenbergi* (Bolli); **(d)** *Globanomalina pseudomenardii* (Bolli); **(e)** *Globanomalina* cf. *chapmani* (Parr); **(f–h)** *Subbotina triloculinoides* (Plummer); **(i)** *Morozovella angulata* (White); **(j)** *Morozovella occlusa* (Loeblich & Tappan); **(k)** *Morozovella aequa* (Cushman & Renz); **(l)** *Morozovella* cf. *aequa* (Cushman & Renz); **(m)** *Planktonic foraminifera*; **(n–p)** *Planorbulina? antiqua* Mangin; **(r,s)** *Stomatorbina? binkhorsti* Reuss; **(t)** *Stomatorbina* sp.; **(u)** *Sistanites iranicus* Rahaghi; **(v)** *Valvulineria paralensis* Cushman; **(w–y)** *Valvulineria bacetai* Serra-Kiel & Vicedo; **(z)** *Idalina sinjarica* Grimsdale; **(x_1)** *Idalina* sp.; **(y_1)** *Coskinon rajkae* (Hottinger & Drobne); **(z_1)** Corallinaceae; **(x_2)** *Dendrophyllia* sp.

In the breccias of the lower part of the succession at the Bahori–Gornja Bodežišta profile (Fig. 10; location 7, Sample No. 57/1), a reworked Maastrichtian microfaunal assemblage was identified, including *Orbitoides media* (d'Archiac), *Orbitoides* cf. *apiculata* Schlumberger (Fig. 6u), *Siderolites calcitrapoides* Lamarck (Fig. 6v,y), *Lepidorbitoides* cf. *socialis* (Leymerie) (Fig. 6w), together with rare Paleocene foraminifera such as *Sistanites iranicus* Rahaghi (Fig. 9u). In biomicrites (Fig. 10; location 7, Sample No. 57/2), rare *Morozovella angulata* (White), *Morozovella* cf. *aequa* (Cushman & Renz), and *?Acarinina* sp. were identified. This assemblage indicates a Selandian–Thanetian age.

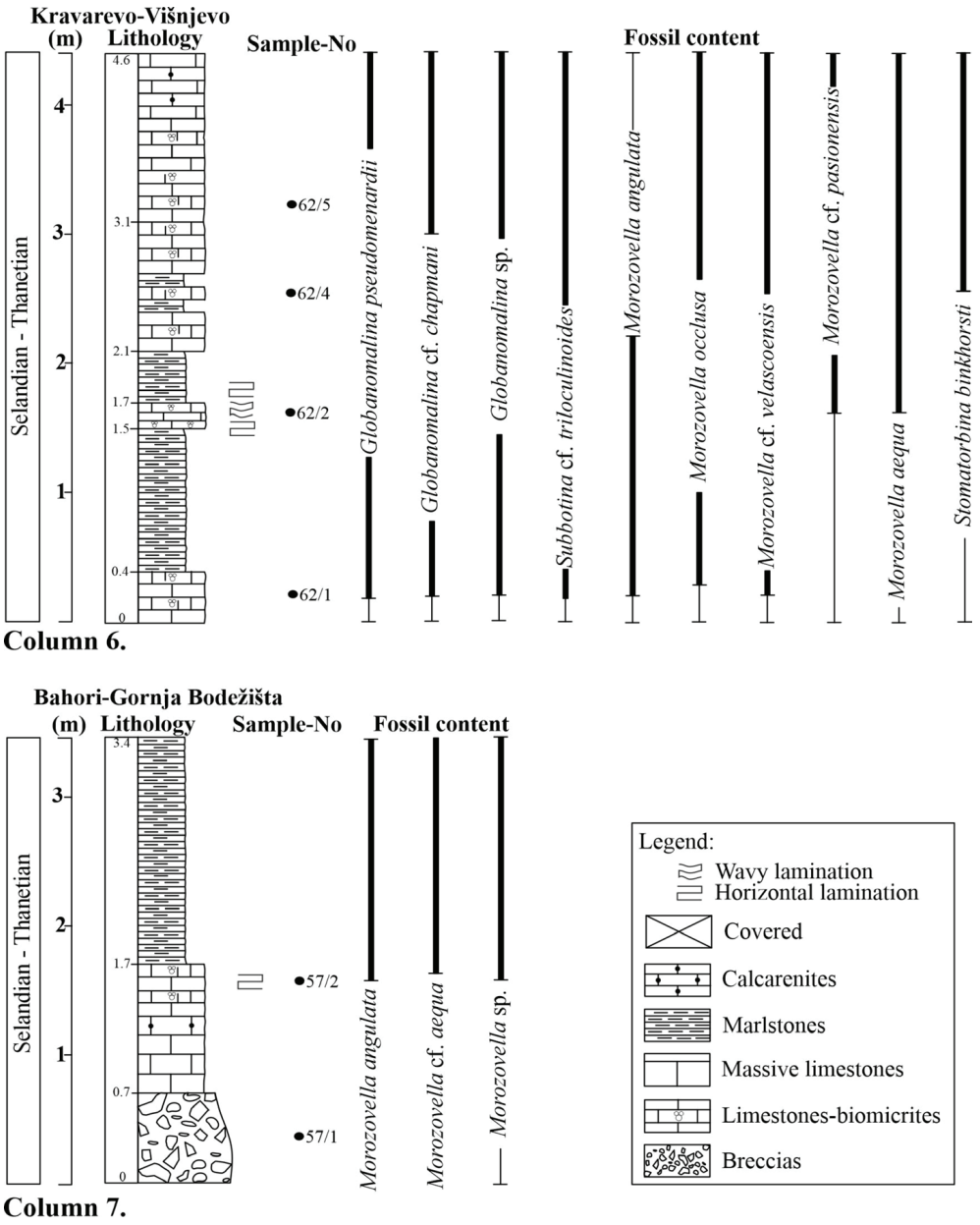

Fig. 10. Geological sections of the carbonate–clastic Paleogene succession of the Ugar Formation: **(a)** Kravarevo–Višnjevo profile; **(b)** Bahori–Gornja Bodežišta profile.

Carbonate–siliciclastic Paleocene sediments were also studied along local road sections near Desivoje Lake, the village of Dražljevo, Kljeuta, and Gornja Bodežišta. At the Desivoje Lake locality (Fig. 2; location 19, Sample No. 19), planktonic fossils and various benthic bioclasts (foraminifers, bryozoans, echinoderms) were identified. The assemblage includes *Globanomalina* cf. *archeocompressa* (Plummer) (Fig. 9a), *Planorbulina? cretae* (Marsson) (Fig. 6x$_1$), *Valvulineria patalaensis* Haque (Fig. 9v) (see Supplementary Table S2) of Danian–early Selandian (?) age.

Calcareous nannofossils were also identified, including *Chiasmolithus danicus* (Brotzen 1959), Hay & Mohler 1967 (Fig. 5-7), *Toweius* sp. (Fig. 5-9), *Coccolithus pelagicus* (Wallich 1877), Schiller 1930 (Fig. 5-10), *Prinsius martini* (Perch-Nielsen 1969), Haq 1971 (Fig. 5-11), *Sphenolithus* cf. *moriformis* (Brönnimann & Stradner 1960), Bramlette & Wilcoxon 1967 (Fig. 5-13), *Ericsonia subpertusa* Hay & Mohler 1967 (Fig. 5-15), *Prinsius bisulcus* (Stradner 1963), Hay & Mohler 1967 (Fig. 5-16), *Ellipsolithus distichus* (Bramlette & Sullivan 1961), Sullivan 1964 (Fig. 5-21), *Lithoptychius* sp. (Fig. 5-22), *Fasciculithus billii* Perch-Nielsen 1971 (Fig. 5-23), *Fasciculithus involutus* Bramlette & Sullivan 1961 (Fig. 5-27), *Neochiastozygus* cf. *concinnus* (Martini 1961), Perch-Nielsen 1971 (Fig. 5-28), *Tectulithus pileatus* (Bukry 1973), Miniati et al. 2021 (Fig. 5-29). This assemblage suggests a Selandian age.

At the villages of Dražljevo and Kljeuta (Fig. 2; location marked as Sample No. 26), Cretaceous benthic and planktonic foraminifera were identified in various breccia limestone fragments. The assemblage includes *Orbitoides media* (d'Archiac) (Fig. 6s), *Orbitoides* cf. *apiculata* Schlumberger, *Lepidorbitoides socialis* (Leymerie) (Fig. 6t), *Nezzazatinella picardi* (Henson), *Minouxia lobata* Gendrot, and the coralline alga *Melobesia* sp., followed by *Hedbergella* sp., *Whiteinella* sp., *Pithonella sphaerica* (Kaufmann) and *Bonetocardiella* sp. These fossils range in age from the Turonian to the Maastrichtian. Other biomicrite fragments contain *Decastronema kotori* (Radoičić) (Fig. 6m), as well as *Globotruncanita stuartiformis* (Dalbiez), *Radotruncana* cf. *subspinosa* (Pessagno), and *Marginotruncana* sp., indicating a Campanian age.

The presence of *Bonetocardiella conoidea* (Bonet) (Fig. 6k) and the Maastrichtian species *Siderolites calcitrapoides* Lamarck in the limestone breccia west of the Mušnica River (Fig. 2; Sample No. 37) suggests that the formation of the breccia could range from the latest Maastrichtian to the Paleocene. In the biomicrites west of the Mušnica River, the following fossils were identified: *Planorbulina? antiqua* Manguin (Fig. 9n), *Morozovella* sp., *Dendrophyllia* sp. corals (Fig. 9x$_1$), and the dasyclad alga of *Microsporangiella* sp., indicating Paleocene age.

At Gornja Bodežišta (Fig. 2; location marked as Sample No 64/1), both benthic and planktonic foraminifera of Maastrichtian age were identified in biocalcarenites, including *Valvulina triangularis* d'Orbigny, *Contusotruncana fornicata* (Plummer) (Fig. 6h), *Globotruncanita stuartiformis* (Dalbiez), *Hellenocyclina beotica* Reichel, *Fleuryana adriatica* De Castro, Drobne & Gušić (Fig. 6z), *Orbitoides* cf. *media* (d'Archiac), *Rotalia trochidiformis* (Lamarck), *Planoglobulina* cf. *acervulinoides* (Egger).

The overlying biosparites (Fig. 2; location marked as Sample No. 64/3) are composed of bryozoan bioclasts, reworked rudist fragments, Orbitolinidae, and other Upper Cretaceous foraminifera, including *Globotruncanita stuarti* (Lapparent), *Globotruncanita* cf. *stuartiformis* (Dalbiez), *Contusotruncana fornicata* (Plummer), *Hellenocyclina beotica* Reichel, etc. These are associated with *Planorbulina? antiqua* Manguin (Fig. 9o), *Planorbulinella dordoniensis* Hofker, *Cibicidoides succedens* (Brotzen), and *Coskinon rajkae* (Fig. 9y$_1$), indicating Selandian age. In recrystallized biosparites (Sample No. 64/5), the following taxa were identified: *Cibicidoides succedens* (Brotzen), *Pararotalia* sp., *Coskinon* sp. This assemblage suggests an early Paleocene age.

Fold structures and fault kinematics in the Gacko area

Structural–tectonic analysis of folds and faults within the Vranduk and Ugar formations was carried out to identify the principal deformation phases that controlled the structural evolution of the Bosnian Flysch domain.

Cretaceous–Paleogene NE–SW-oriented compression axis (D1)

Field investigations revealed numerous meter-to decametre-scale folds of variable geometries within the Vranduk Formation. These are predominantly overturned to recumbent, southwest-vergent folds (Fig. 11a–f).

Characteristic fold geometries observed in the Vranduk Formation are also reflected in the statistical bedding diagram (Fig. 11e). The plotted bedding data indicate frequently measured steep and inverted limbs of overturned, recumbent, and asymmetric southwest-vergent folds.

Stratified breccias, limestones, calcarenites, and marls of the Ugar Formation are likewise folded into meter-scale asymmetric folds, characterized by subvertical to overturned geometries. The axial planes of these folds are inclined and show predominant southwest vergence (Fig. 11f–j). The contour diagram of bedding attitudes in the Ugar Formation documents asymmetric overturned and symmetrical south-vergent folds with NW–SE-oriented axes (Fig. 11h).

All observed structures affect within Cretaceous–Paleogene sediments, which facilitates the interpretation of the timing of their activity. Initially, reverse faults with SE–NW strike and pronounced southwest vergence were formed, along which tectonic transport toward the southwest was inferred. Observed local reverse structures are part of a regional thrust that includes prominent reverse faulting-related features in the studied area (Fig. 12a, b and d).

Progression of compression and shortening within the area was accompanied by the development of reverse NNE–SSW striking faults, along which, due to SW dipping geometry, tectonic transport was directed toward the northeast (Fig. 12b, d). In the study area, strike-slip fault surfaces are common, with the compression axes oriented NE–SW (Fig. 12c). Based on our field observations and regional studies (van Unen et al. 2019), these faults likely formed during Cretaceous–Paleogene orogenic shortening or immediately thereafter.

Oligocene–Miocene bi-directional extension (D2)

The second observed deformation phase incorporates normal faults developed under extensional conditions with variably oriented extension axes (Fig. 12e–h). Spatial and kinematic analyses of faults within the studied structures suggest fault activity under an extensional stress field, both parallel and perpendicular to the orogen strike. The extension axis, parallel to the orogen strike is oriented SE–NW, with faults striking NE–SW (Fig. 12e). The extension axis, perpendicular to the orogen strike is oriented NE–SW, with faults striking NW–SE (Fig. 12f). Additionally, numerous normal structures and sliding fractures with centimeter-scale displacements have been observed in Neogene deposits, formed together under extension parallel to the orogen strike (Fig. 13a–f).

Late Miocene–Recent N–S to NNE–SSW-oriented compression/transpression axis (D3)

The third deformation phase encompasses structures that were active under compression and transpression affecting the entire Dinarides from the latest Neogene through the Quaternary (Andrić et al. 2017). Redistribution of the regional stress field led to the reactivation of preexisting structures and the local formation of new faults at various orientations, exhibiting reverse and strike-slip kinematics. Numerous

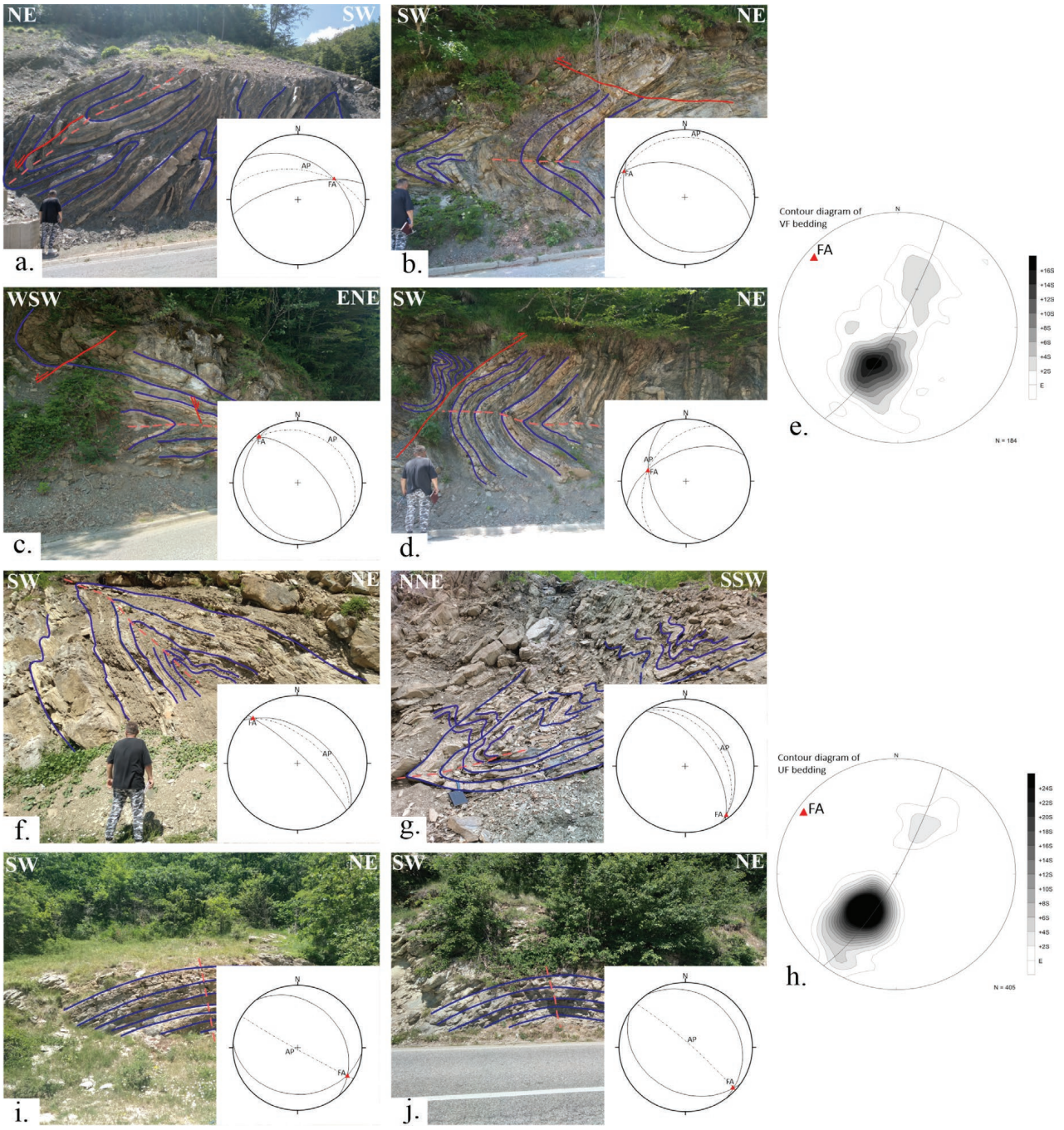

Fig. 11. Fold structures observed in the Vranduk and Ugar formations: **(a)** Southwest-vergent overturned fold in the Vranduk Formation; **(b–d)** Southwest-vergent recumbent fold in the Vranduk Formation; **(e)** Statistical diagram of bedding observed in the sediments of the Vranduk Formation. The contour diagram of bedding reveals an elongated maximum, with a fold axis striking NW–SE; **(f)** Southwest-vergent inclined overturned fold in the Vranduk Formation; **(g)** Southwest-vergent overturned fold in the Ugar Formation; **(h)** Northeast-vergent normal fold in the Ugar Formation; **(i)** Southwest normal fold in the Ugar Formation; **(j)** Statistical diagram of bedding observed in the sediments of the Ugar Formation. The contour diagram of bedding reveals an elongated maximum, with a fold axis striking NW–SE. Fold are affected by local fractures (red lines at photos); FA – Fold axis; AP – Axial plane. Axial plane is shown by a red dashed line in the figures.

oblique-slip fault, including dextral N–S-striking faults, were active within the NE–SW-oriented compression axis (Fig. 14a). Additionally, NE–SW-striking strike-slip faults were active under N–S-oriented transpression/transtension axis (Fig. 14b_1), NW–SE-striking strike-slip faults under NNE–SSW-oriented compression axis (Fig. 14c), and NE–SW-striking reverse faults under NW–SE-oriented compression axis (Fig. 14d). NE–SW-striking strike-slip faults active within the transpressional/transtensional stress field are associated with an N–S oriented P-axis, which may be suggested also for N–S-striking strike-slip faults (Fig. 14b_2).

In the Neogene sediments of the Gacko Basin, structures active under compressional and transpressional tectonic regimes have been observed. In the areas affected by transpression, flower structures can also form (Fig. 14e). The diagram (bottom left, Fig. 14e_1) illustrates NE–SW-striking strike-slip faults active under NE–SW-oriented compression axis, which are kinematically incompatible with NW–SE-striking faults. The diagram (bottom right, Fig. 14e_2) shows strike-slip faults striking NE–SW active under the NW-SE-oriented compression axis. During these deformation phases, pre-existing faults were predominantly reactivated. Figure 14f shows an oblique-slip fault, which, based on shear sense and folding of the host layer, was originally a gravitational fault (blue arrow in the Fig. 14f) that became reactivated as an oblique-slip fault. Initially, these faults were formed as normal faults under an extensional tectonic regime and were later reactivated under a transpression and compressional regime.

Discussion

Lithostratigraphic properties of the Vranduk and Ugar formations

In the area of eastern Herzegovina, the Vranduk Formation is composed of a sandy-marly series that exhibits turbidite characteristics (Dimitrijević et al. 1968; Hrvatović 2022 and references therein). Petrographic characteristics indicate that the Vranduk Formation predominantly consists of sandstones showing a mixed siliciclastic–carbonate composition, ranging from quartz-rich litharenites to quartz-poor calcareous litharenites. Most litharenite samples contain fragments of basic volcanics, diabase with ophitic texture, and serpentinites with a mesh texture, suggesting that the clasts of the Vranduk Formation largely originated from ophiolites. Previous research indicates that the sediments of the Vranduk Formation were derived from magmatic rock complexes (diabases and spilites), serpentinites, quartzites, and Jurassic to lowermost Cretaceous limestones, as evidenced by lithoclasts in polymictic breccias and by heavy mineral assemblages (Dimitrijević et al. 1968; Mikes et al. 2008). The onset of sedimentation of the Vranduk Formation is not well defined because the formation contains sediments lacking direct age-diagnostic fossils (Mikes et al. 2008). Based on calpionellid and foraminiferal assemblages, the age of the Vranduk Formation in Central Bosnia is generally considered to range from the Tithonian to the Berriasian–Valanginian (Charvet 1978; Olujić 1978). The upper parts of the Vranduk Formation in the Bosna River section contain a diverse Lower Cretaceous assemblage, including *Braarudosphaera africana* (Aptian to Cenomanian), suggesting that the age of this sample cannot be older than Aptian (Mikes et al. 2008). The northern equivalent of the Vranduk Formation in the Dinarides is the Tithonian–Albian Oštrc Formation on Ivanšica Mountain in northern Croatia (e.g., Lužar-Oberiter et al. 2009). Our research in the area of eastern Herzegovina suggests that, if the limestone clasts within the breccias and conglomerates are older than the enclosing rudite matrix, due to potential reworking of some fossils from shallower to deeper marine environments, then the upper stratigraphic levels of the Vranduk Formation in the study area could be of post–Lower Aptian age, possibly corresponding to the Upper Aptian or even Albian. This interpretation is supported by Albian calcareous nannofossil assemblages identified in samples collected near Čemerno (Fig. 2; Sample No. 39). Previously, the age of these breccias was considered Jurassic based on larger benthic foraminifera (Dimitrijević et al. 1968).

Sedimentation of the Ugar Formation in eastern Herzegovina, near Gacko, begins with a basal series of breccias and conglomerates of variable thickness. This basal unit is thin and is interpreted as the result of rapid deposition, as indicated by its coarse and poorly sorted clasts. The basal breccias and conglomerates do not exhibit turbidite features, suggesting that these deposits were produced by sediment gravity flows. Biostratigraphic analysis of planktonic foraminifera from the basal breccias and conglomerates indicates an age ranging from the possible uppermost Turonian to the lower Santonian. However, more recently, this breccia interval has been interpreted as the base of a Late Cretaceous transgression, possibly a transgressive succession characterized by shallow marine deposits followed by rapid deepening of the depositional environment (Lužar-Oberiter et al. 2023). In contrast, Cadet & Sigal (1969) attributed the beginning of the transgression to the Cenomanian.

The basal breccias and conglomerates of the Ugar Formation are overlain by a series of Upper Cretaceous carbonate–clastic rocks. Large amounts of material were transported into the basin by gravity flows. As sedimentation depth increased, bioclastic micritic limestones were deposited (Božović et al. 2024). Packages of carbonate breccias are cyclically repeated and are interpreted as the product of syndepositional tectonic activity, indicating deposition in the tectonically controlled foreland basin (Lužar-Oberiter et al. 2023; Šamarija et al. 2025). Between the carbonate breccias, micritic limestones, and marly limestones occur intervals of grading, horizontal laminations, and oblique and wavy flow laminations, with lenses of bioclasts. The microfauna of this series is indicative of the Upper Santonian to Maastrichtian. Locally, biostratigraphic data indicate these are carbonate turbidites of Maastrichtian age that have been tectonically transported reversely along the internal nappe (Fig. 2; Samples Nos. 52, 54, 55).

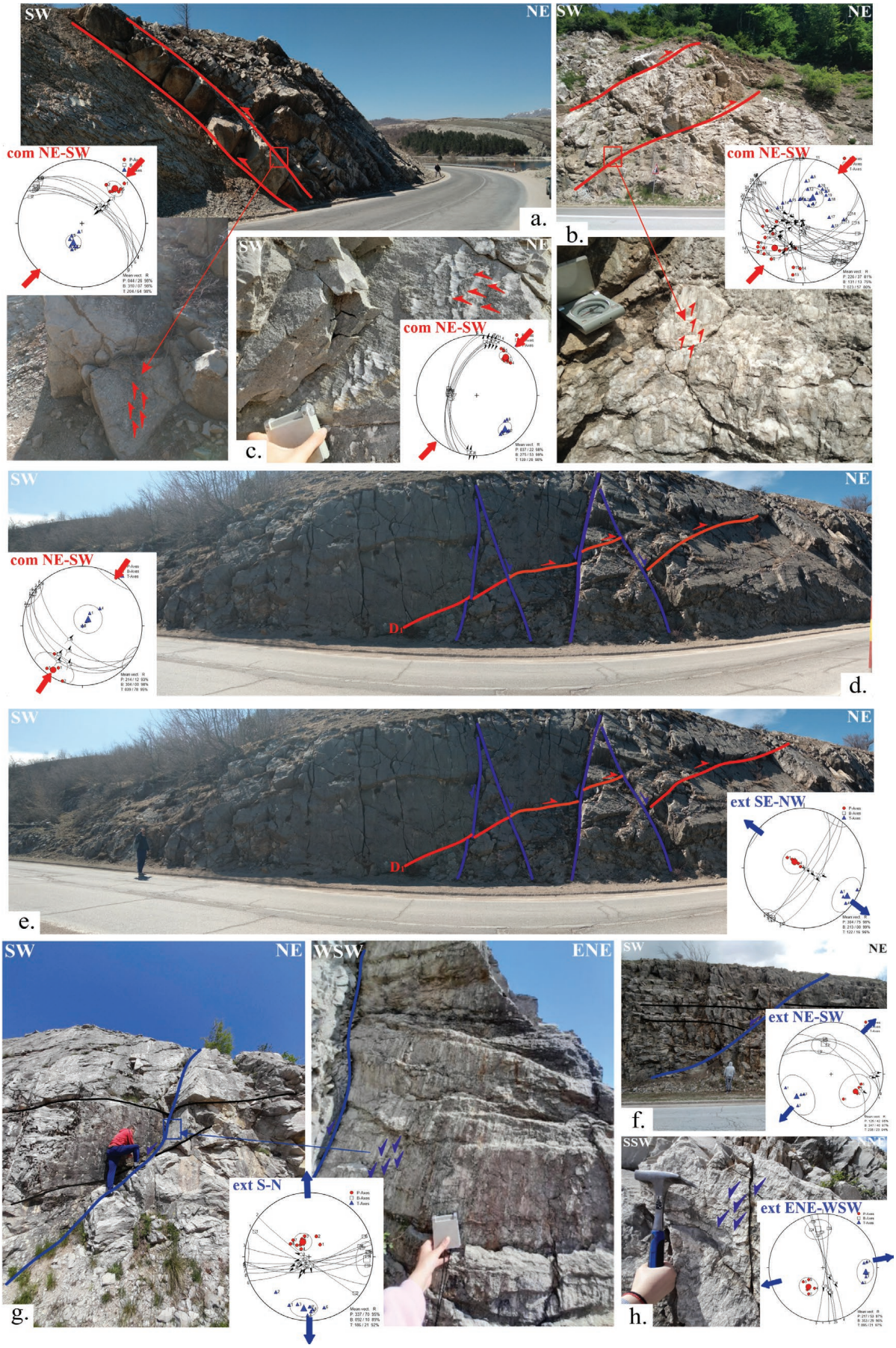
SW
NE
com NE-SW
a.
b.
c.
D1
d.
e.
ext SE-NW
WSW
ENE
ext S-N
f.
ext NE-SW
SSW
ext ENE-WSW
g.
h.

Fig. 12. Reverse and strike-slip faults active during Cretaceous–Paleogene compression, dipping towards NE (a–d) and normal faults active during extension parallel to the orogen strike, and structures active in extension perpendicular to the orogen strike (e–h): **(a)** Reverse faults dipping to the northeast; **(b)** Reverse faults dipping to the southwest; **(c)** Striations on a dextral strike-slip fault belonging to the group of transfer structures; **(d)** Reverse faults dipping to the southwest, overprinted by younger normal faults; **(e)** Normal faults active in extension parallel to the orogen strike have SW–NE-oriented extension, with faults striking NW–SE; **(f)** Extension perpendicular to the orogen strike is oriented NW–SE, with faults striking SW–NE; **(g)** Normal faults active during the subphase of extension parallel to the orogen. The extension axis is oriented N–S; **(h)** Striations on a normal faults active during the subphase of extension perpendicular to the orogen. The extension axis is oriented E–W.

Data from this study indicate that the broadest belt around Gacko in eastern Herzegovina, is composed of a Paleocene carbonate–siliciclastic succession, including carbonate breccias, sandy limestones, marly limestones, calcarenites, and marls. This succession is characterized by well-developed grading in coarse-grained intervals and laminations that are horizontal, oblique, wavy, and convolute in the fine-grained sediment intervals (Supplementary Fig. S2a, b). Paleocene siliciclastic–carbonate deposits contain sedimentary structures, current-induced markings, and trace fossils preserved within a large-scale slump structures. Paleotransport directions indicate that the material was transported from the W–SW (Dimitrijević et al. 1968). These features suggest that gravity currents of varying density and transport mechanisms influenced this part of the series (Mudler & Alexander 2001). This Paleocene series represents the proximal part of the Upper Cretaceous–Paleogene turbidite sequence (Hrvatović 2022). The siliciclastic component of the sandstones in the Ugar Formation is largely composed of quartz and foliated quartz–mica lithoclasts, while the heavy mineral fraction includes Cr-spinel, zircon, garnet, rutile, and tourmaline, indicating contributions of material from units exposed in the advancing orogenic wedge (Lužar-Oberiter et al. 2023). Although most authors, except for Dimitrijević et al. (1968), interpret the Ugar Formation as Upper Cretaceous in age, biostratigraphic analyses conducted during this study indicate that the majority of the unit is Paleocene in age.

Implications for the tectonic evolution of the Vranduk and Ugar formations

Three significant and temporally distinct tectonic phases have been defined by tectonic studies, spanning from the Cretaceous period to the present. The first deformation phase resulted from prolonged convergence during continental collision, which led to the formation of southwest-vergent nappes and northeast-vergent reverse faults (van Unen et al. 2019). Foreland-vergent thrust faults represent the dominant tectonic structures within the foreland basin domain. The development of northeast-vergent back-thrusts, as secondary structures in a compressional regime, likely reflects a late-stage compressional phase, during which continued crustal shortening and wedge thickening led to local stress reorientation and the activation of oppositely verging thrusts (Porkoláb et al. 2019; Schmit et al. 2020; Casini et al. 2025).

The Cretaceous–Paleogene tectonics are characterized by periods of final collision and the closure of the remaining Neotethys Ocean (e.g., Pamić et al. 2002; Schmid et al. 2020). The onset of the Cretaceous–Paleogene collision coincident with the deposition of deep-water syn-contractional Campanian–Maastrichtian turbidites, which localized deformation during thrusting (Demir et al. 2019). The Cretaceous–Paleogene tectonics involved compressional phases driven by the subduction of the Adriatic plate and collision with units of European affinity, manifested by multiphase folding, as well as activation of large nappes and reverse faults (van Unen et al. 2019). The predominant faults are NW–SE–striking reverse faults, which were active under NE–SW–oriented compression axis (Fig. 11a, b, and d). In the stress field of the same orientation, NNW–SSE strike-slip faults were also active (Fig. 11c). Structures active under NE–SW, NNE–SSW to N–S-oriented compression axis developed during the compressional Cretaceous–Paleogene collision period (van Unen et al. 2019). Porkoláb et al. (2019) note that during the collision of the Adriatic plate with European affinity units, the predominant compression direction was NE–SW.

The second deformation phase was associated with a significant regional event, the Oligocene–Miocene extension, during which older reverse structures were reactivated as normal faults, and new normal faults also developed (e.g., Toljić et al. 2013 with references; van Unen et al. 2019). Besides the Dinarides, the Alpine pro-foreland, i.e., the German Molasse Basin, shows a similar reactivation pattern, with deformation recorded along reactivated Mesozoic faults as well as newly formed Cenozoic normal faults (Eskens et al. 2025). In this Oligocene–Miocene extensional pattern, two groups of (re)activated normal faults have been distinguished. The first group includes NE–SW striking structures, active in extension parallel to the orogen strike. The second group, NW–SE-oriented faults, was active in extension perpendicular to the orogen. It is well established that flexural basins commonly develop gravity faults both parallel and perpendicular to the basin's long axis (Tavani et al. 2015). Such faults may therefore share the characteristics attributed here to the Oligocene–Miocene structures. Given that similarly oriented and kinematically comparable faults are documented in the Neogene sediments of the Gacko Basin in eastern Herzegovina, the normal faults discussed here are interpreted as Oligocene–Miocene in age.

The structures formed during the Oligocene–Miocene extension migrated both temporally and spatially and were subjected to clockwise rotation. As a result of orogenic rotation within an extensional stress field, two fault subgroups developed with slightly different orientations, both formed

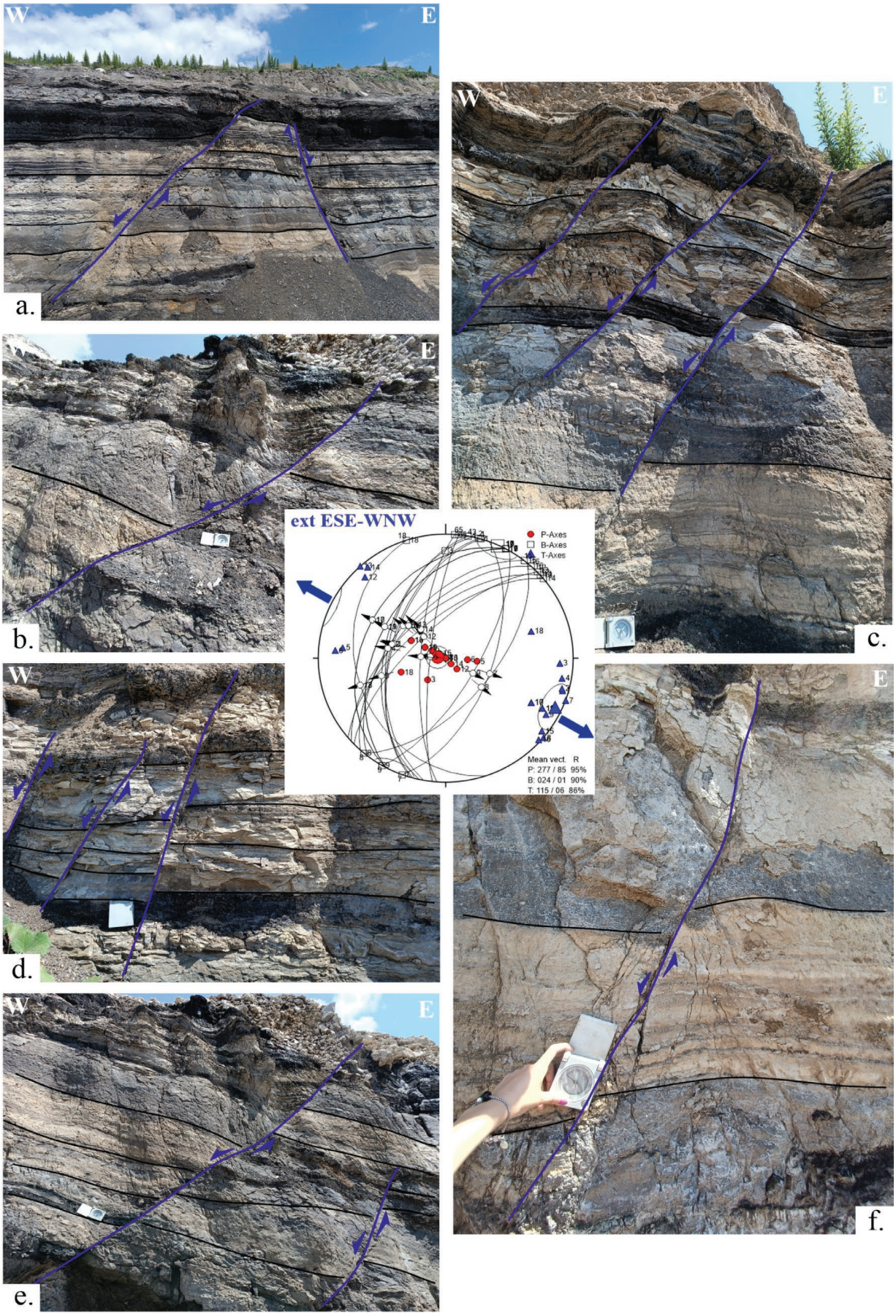
W
E
a.
b.
c.
d.
e.
f.
ext ESE-WNW
P-Axes
B-Axes
T-Axes
Mean vect. R
P: 277 / 85 95%
B: 024 / 01 90%
T: 115 / 06 86%

Fig. 13. Normal faults observed in the Neogene sediments of the Gacko Basin: **(a)** Normal faults activated during WNW–ESE oriented extensional regime; **(b)** Normal fault activated during NW–SE oriented extensional regime; **(c)** Local normal structures activated during ESE–WNW oriented extensional regime; **(d)** Local normal structures activated during NW–SE oriented extensional regime; **(e)** Normal faults activated during ESE–WNW oriented extensional regime; **(f)** Local normal structure activated during NW–SE oriented extensional regime. The diagram demonstrates that these structures were developed in extension parallel to the orogen strike.

during the second deformation phase. The first subgroup, comprising E–W striking faults, was active in extension parallel to the orogen strike (Fig. 12g). The second subgroup, consisting of N–S striking faults, was active in extension perpendicular to the orogen strike (Fig. 12h). Perpendicular extension is attributed to the rollback of the subducted oceanic lithosphere in the Carpathians and to the presence of oceanic crust beneath the Dinarides (Handy et al. 2015 with references). Parallel extension is linked to the Carpathian subduction and the detachment of the Adriatic plate, and may have been further influenced by rollback in the Aegean subduction zone (Handy et al. 2015 and references therein). Additionally, van Unen et al. (2019) associate Miocene extension with subduction during plate separation or with post-detachment gravitational collapse of the orogen.

Similar structures have been described in other parts of the Dinarides. The Oligocene–Miocene extension created numerous normal faults along the major Dinaric contacts (van Unen et al. 2019). In the external and internal Dinarides (Fig. 1b), paleostress studies indicate the existence of a bivergent extension regime (van Gelder et al. 2015; Žibret & Vrabec 2016; Porkoláb et al. 2019). Structural and geodynamic studies have shown that extension in the southern part of the Pannonian Basin was largely driven by regional clockwise rotation of the Tisza–Dacia block (Horváth et al. 2015). Conversely, the northern margin of the Dinarides adjacent to the Pannonian Basin experienced extensive exhumation in E–W oriented extension (Ustaszewski et al. 2010; Toljić et al. 2013; van Gelder et al. 2015). Additionally, Horváth et al. (2015) and Matenco & Radivojević (2012) linked the Oligocene–Miocene extension to the opening of the extensional Pannonian Basin. The opening was initiated around 20 Ma, between the subducted Adriatic and Carpathian oceanic lithosphere, as a result of slab retreats (Horváth et al. 2015). The Oligocene–Miocene extension also led to the formation of intramontane Dinaric lakes, including the Gacko Neogene Basin (Krstić et al. 2003; Neubauer et al. 2003; Harzhauser & Mandić 2008; de Leeuw et al. 2010; Mandić et al. 2011).

The extension phase was followed by compression and inversion of Neogene basins, which began in the late Miocene and remains active today. This phase of tectonic deformation resulted from the indentation and northward to north-northeastward movement of the Adriatic plate (Schmid et al. 2020) coupled with the counterclockwise rotation of the Adriatic plate (Márton et al. 2003; Weber et al. 2010; Heidbach et al. 2016; van Unen et al. 2019). The youngest deformation phase is characterized by N–S oriented compression in a transpressional and reverse tectonic regime. Paleostress analysis results indicate that the N–S oriented compression gradually changes orientation towards NNE–SSW and NE–SW in the southeastern Dinarides (Bada et al. 2007; Heidbach et al. 2007).

Conclusion

The study of the evolution of the Cretaceous–Paleocene foreland basin in eastern Herzegovina, through field investigations combined with biostratigraphic age determinations, has shown that this part of the Dinaric chain was influenced by a multi-phase tectonic evolution. Sedimentological and biostratigraphic data indicate that the Bosnian Flysch Units have a complex organization and are the product of tectonically controlled Cretaceous–Paleogene deposition and deformation.

Sedimentological evidence indicates that the Vranduk Formation in eastern Herzegovina is predominantly clastic in nature, sourced from the northeast continental basements composed of metamorphic and ophiolitic rocks. Biostratigraphic data suggest Barremian–Lower Aptian to post-Lower Aptian age for the Vranduk Formation in this area.

The Ugar Formation in eastern Herzegovina consists of three members: (1) basal Upper Cretaceous limestone breccias and conglomerates; (2) Upper Cretaceous carbonate–clastic sediments; and (3) Paleocene carbonate–siliciclastic sediments, derived from the southwestern situated Adriatic Carbonate Platform, and redeposited into the turbiditic basin. Biostratigraphic studies support a possible uppermost Turonian to lower Santonian age for the basal breccias and conglomerates, Upper Santonian to Maastrichtian age of Upper Cretaceous carbonates, and Paleocene age of carbonate–siliciclastic sediments.

Structural investigations reveal that both formations exhibit complex folding, with overturned, recumbent, and asymmetrical folds verging southwest, formed during NE–SW compressional phases associated with Cretaceous and Paleogene shortening and thrusting.

Kinematic analysis of faults and the reconstruction of paleostress fields have identified three significant and temporally distinct tectonic phases. The oldest deformation phase is represented by a group of reverse and strike-slip faults active in the NE–SW-oriented compression axis. Initially, reverse faults trending NW–SE formed, along which tectonic transport occurred toward the southwest. In front of these thrust structures, a long-lived regional foreland basin developed where Cretaceous-Paleocene formations were deposited. The culmination of continental collision resulted in the development of a group of NW–SE trending reverse faults, with tectonic transport directed toward the northeast.

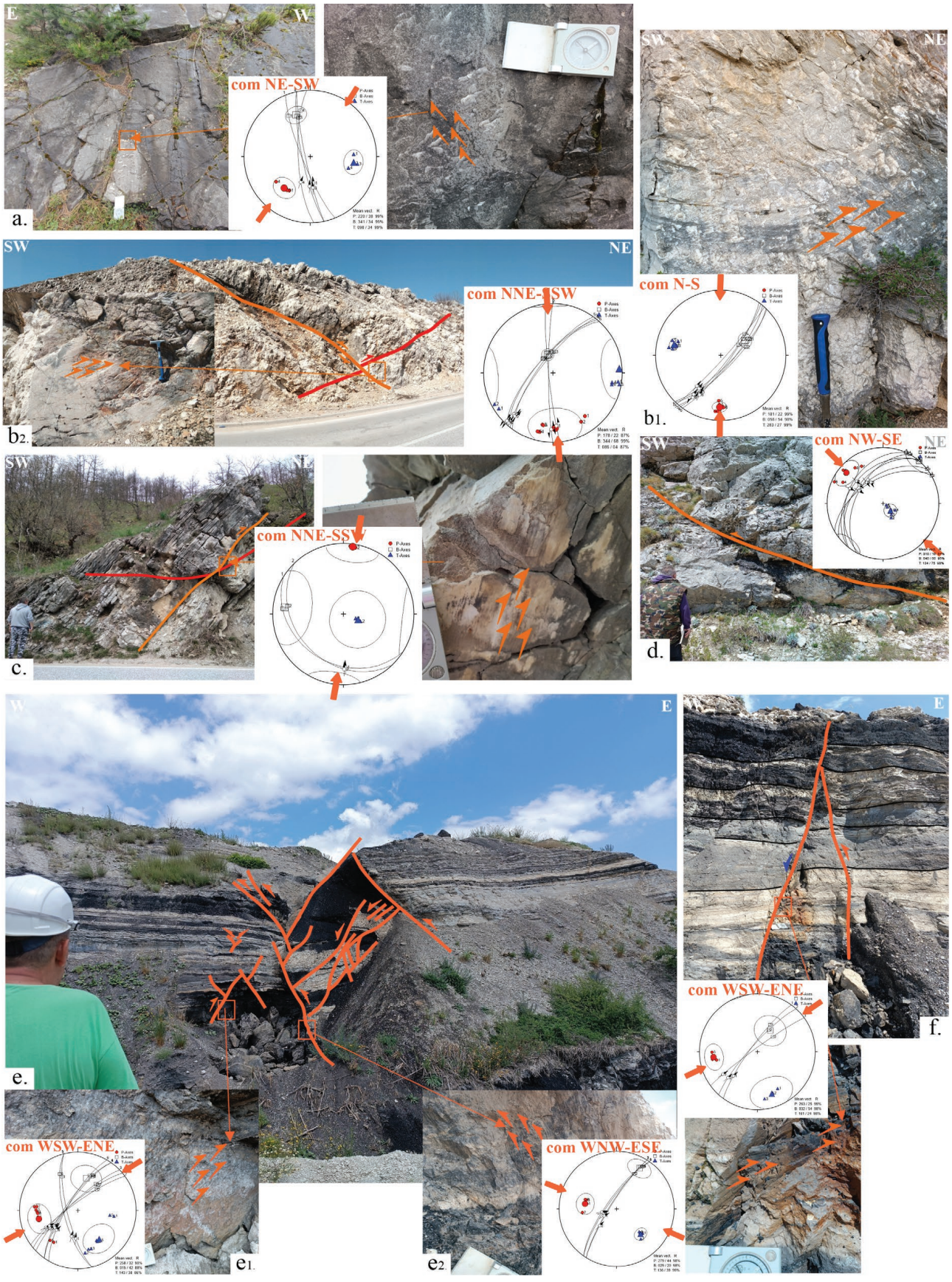
E
W
com NE-SW
a.
SW
NE
com N-S
b1.
SW
NE
com NNE-SSW
b2.
SW
com NNE-SSW
c.
SW
NE
com NW-SE
d.
W
E
com WSW-ENE
e.
com WSW-ENE
e1.
com WNW-ESE
e2.
E
com WSW-ENE
f.

Fig. 14. Reverse and strike-slip faults activated under different stress regimes during the compressional tectonic phase in the Late Neogene (a–d) and reactivated reverse faults, active under compressional and transpressional tectonic regimes in the Neogene sediments of the Gacko Basin (e, f): **(a)** Reverse faults striking N–S, active during NW–SE oriented compression; **(b_1)** Reverse faults striking NE–SW, active during N–S oriented compression; **(b_2)** Strike-slip faults active during N–S oriented compression; **(c)** Reverse faults striking NW–SE, active during NNE–SSW oriented compression; **(d)** Reverse faults striking NE–SW, active during NW–SE oriented compression; **(e)** Inversion structure exhibiting attributes of a flower structure; **(e_1)** Strike slip faults active during NE–SW oriented compression and reverse faults striking NNW–SSE active during NE–SW oriented compression; **(e_2)** Strike-slip faults striking NE–SW, active during NW–SE oriented compression. Figures 14e_1 and 14e_2 show zoom-ins of Fig. 14e. **(f)** Oblique-slip faults active during NE–SW oriented compression.

In the broader context of the tectonic evolution of the Dinarides, a set of normal faults formed during the second deformation phase as a result of regional extension. Structures active in extension parallel to the orogen (NW–SE orientation) and those active in extension perpendicular to the orogen (NE–SW orientation) can be distinguished. The youngest deformation phase involved faults active in compression that affected the entire Dinarides in the Late Neogene. This stress field was characterized by reverse and strike-slip faults active under N–S to NNE–SSW-oriented compression/transpression axis.

Finally, deposition of the Vranduk and Ugar Formations took place in a foreland basin and was driven by nappe propagation and displacement towards the foreland in response to ongoing compression.

Acknowledgements: This study was supported by the Ministry of Science, Technological Development and innovation of the Republic of Serbia, Contract on realization and financing of scientific research of SRI in 2025, No. 451-03-136/2025-03/200126. Lucas H.J. Eskens and an anonymous reviewer are gratefully acknowledged for comments and suggestions, which significantly improved the quality of this manuscript. The authors are grateful to editor Rastislav Vojtko for guidance and constructive comments and suggestions.

References

Andrić N., Sant K., Matenco L., Mandic O., Tomljenović B., Pavelić D., Hrvatović H., Demir V. & Ooms J. 2017: The link between tectonics and sedimentation in asymmetric extensional basins: Inferences from the study of the Sarajevo–Zenica Basin. *Marine and Petroleum Geology* 83, 305–332. https://doi.org/10.1016/j.marpetgeo.2017.02.024

Angelier J. 1979: Determination of the mean principal directions of stresses for a given fault population. *Tectonophysics* 56, T17–T26. https://doi.org/10.1016/0040-1951(79)90081-7

Aubouin J., Blanchet R., Cadet J. P., Celet P., Charvet J., Chorowicz J., Cousin M. & Rampnoux J. P. 1970: Essai sur la géologie des Dinarides. *Bulletin de la Société Géologique de France* 12, 1060–1095.

Babič Lj. & Zupanič J. 2008: Evolution of a river-fed foreland basin fill: the North Dalmatian flysch revisited (Eocene, Outer Dinarides). *Natura Croatica* 17, 357–374.

Bada G., Horváth F., Dövényi P., Szafián P., Windhoffer G. & Cloetingh S. 2007: Presentday stress field and tectonic inversion in the Pannonian basin. *Global and Planetary Change* 58, 165–180. https://doi.org/10.1016/j.gloplacha.2007.01.007

Balling P., Tomljenović B., Schmid S. & Ustaszewski K. 2021: Contrasting along-strike deformation styles in the central external Dinarides assessed by balanced cross-sections: Implications for the tectonic evolution of its Paleogene flexural foreland basin system. *Global and Planetary Change* 205, 1–24. https://doi.org/10.1016/j.gloplacha.2021.103587

Blanchet R. 1966: Sur l´âge tithonique-éocrétacé d´un flysch des Dinarides internes en Bosnie: le flysch de Vranduk (Yougoslavie). *Compte Rendu sommaire des Séances de la Société géologique de France* 10, 401–403.

Blanchet R., Cadet J.P., Charvet J. & Rampnoux J.P. 1970: Sur l'existence d'un important domaine de flysch titonique-crétacé inférieur en Yougoslavie: l'unite du flysch bosniaque. *Bulletin Société Géologique de France* 11, 871–880.

Božović D., Toljić M., Đaković M., Glavaš T. B. & Milić M. 2024: Lithostratigraphy and biostratigraphy of the Upper Cretaceous limestones of Bjelopavlići (Montenegro): contribution to evolution and paleogeography of the Adriatic Carbonate Platform. *Australian Journal of Earth Sciences* 117, 177–193. https://doi.org/10.17738/ajes.2024.001

Cadet J.P. & Sigal J.1969: Sur la stratigraphie et l'extension duflysch éocretacé en Bosnie Hercégovine méridionale. *Compte Rendu sommaire des Séances de la Société géologique de France* 2, 52–53.

Casini G., Saura E., Pavičić I., Pavlin I., Bilić Š., Peytcheva I.& Šumanovac F. 2025: Bauxite Exploration in Fold-Thrust Belts: Insights from the Posušje Region, Bosina and Herzegovina. *Minerals* 15, 415. https://doi.org/10.3390/min15040415

Charvet J. 1978: Géologie des Dinarides au niveau de la transversale de Sarajevo (Yougoslavie). *Publications de la Société géologique du Nord* 2, 1–554.

Conrad A.M. & Clavel B. 2008: A Lithocodium and Bacinella signature of a a late Hauterivian, local microbial event: The Urgonian limestone in South-East France. *Geologica Croatica* 612, 239–250. https://doi.org/10.4154/GC.2008.19

Ćorić S. & Benić J. 2014: First evidence of the Palaeogene age of the Bosnian Flysch Unit (Dinarides, Bosnia and Herzegovina. *Societa Geologica Italiana* 31, 46–47. https://doi.org/10.3301/ROL.2014.38

Csontos L., Gerzina N., Hrvatović H., Schmid S. & Tomljenović B. 2003: Structure of the Dinarides: a working model. *Annales Universitatis Budapestinensis*, *Sectio Geologica* 35, 143–144.

DeCelles P.G. & Giles A.K. 1996: Foreland basin systems. *Basin Research* 8, 105–123. https://doi.org/10.1046/j.1365-2117.1996.01491.x

de Leeuw A., Mandic O., Vranjković A., Pavelić D., Harzhauser M., Krijgsman W. & Kuiper K.F. 2010: Chronology and integrated stratigraphy of the Miocene Sinj Basin (Dinaride Lake System, Croatia). *Palaeogeography, Palaeoclimatology, Palaeoecology* 292, 155–167. https://doi.org/10.1016/j.palaeo.2010.03.040

Demir V., Matenco L., van Unen M. & Hrvatović H. 2019: Understanding the mechanism of the post-middle Miocene inversion in the Central Dinarides: Inferences from the study of the Sarajevo–Zenica and Konjic Basins. In: Book of abstracts. II Congress of Geologists of Bosnia and Herzegovina (with international participation, 2–4. 10. 2019, Laktaši, Bosnia and Herzegovina.

Dimitrijević M.D. 1997: Geology of Yugoslavia. *Geological Institute GEMINI, Special Publication, Belgrade*, 1–187.

Dimitrijević M., Pantić S., Radoičić R. & Stefanovska D. 1968: Litostratigraphic and biostratigraphic columns of the Mesozoic in the Gacko–Sutjeska–Drina area. *Vesnik* 16, 39–87. https://doi.org/10.1130/0091-7613(1990)0182.3.CO;2

Eskens L.H., Andrić-Tomašević N., Kumar A. & Scheck-Wenderoth M. 2025: Spatiotemporal Growth of Seismic Scale Syn-Flexural Normal Faults in the German Molasse Basin. *Basin Research* 37, e70016. https://doi.org/10.1111/bre.70016

Flemings P.B. & Jordan E.T. 1990: Stratigraphic modeling of the foreland basins. Interpreting thrust deformation and litosphere rheology. *Geology* 18, 430–434.

Handy M.R., Ustaszewski K. & Kissling E. 2015: Reconstructing the Alps– Carpathians–Dinarides as a key to understanding switches in subduction polarity, slab gaps and surface motion. *International Journal of Earth Sciences* 1041,1–26. https://doi.org.10.1007/s00531-014-1060-3

Harzhauser M. & Mandić O. 2008: Neogene lake systems of central and South-Eastern Europe: Faunal diversity, gradients and interrelations. *Paleogeography, Paleoclimatology, Paleoecology* 260, 417–434. https://doi.org/10.1016/j.palaeo.2007.12.013

Heidbach O., Reinecker J., Tingay M., Müller B., Sperner B., Fuchs K. & Wenzel F. 2007: Plate boundary forces are not enough: Second- and third-order stress patterns highlighted in the World Stress Map database. *Tectonics* 26, TC6014.

Heidbach O., Custodio S., Kingdon A., Mariucci M.T., Montone P., Müller B., Pierdominici S. et al. 2016: Stress map of the Mediterranean and central Europe 2016. *GFZ Data Service*. https://doi.org/10.5880/WSM.Europe2016

Horváth F., Musitz B., Balázs A., Végh A., Uhrin A., Nádor A., Koroknai B., Pap N., Tóth T. & Wórum G. 2015: Evolution of the Pannonian basin and its geothermal resources. *Geothermics* 53, 328–352. https://doi.org/10.1016/j.geothermics.2014.07.009

Hrvatović H. 2022: Geological guidebook through Bosnia and Herzegovina. *Academy of sciences and arts of Bosnia and Herzegovina*, *Sarajevo* 10, 62–273. https://doi.org/10.5644/D2022.90

Jolović B., Ćorić S., Toholj N. & Mitrović D. 2017: The Paleocene sediments in the Durmitor flysch (The Republic of Srpska, Bosnia and Herzegovina). *Geološki glasnik* 37, 1–32.

Krstić N., Savić L., Jovanović G. & Bodor E. 2003: Lower Miocene lakes of the Balkan Land. *Acta Geologica Hungarica* 46, 291–299. https://doi.org/10.1556/AGeol.46.2003.3.4

Lužar-Oberiter B., Mikes T., von Eynatten H. & Babić Lj. 2009: Ophiolitic detritus in Cretaceous clastic formations of the Dinarides (NW Croatia): evidence from Cr-spinel chemistry. *International Journal of Earth Sciences* 98, 1097–1108. https://doi.org/10.1007/s00531-008-0306-3

Lužar-Oberiter B., Gobo K., Kukoč D., Petrinjak K., Aščić Š., Šamarija R., Kocjančić A., Mrinjek E. & Markotić L. 2023: Mesozoic–Cenozoic Dinaric foreland basins. In: Sedimentary cover of the Adria and its surroundings, 36th International Meeting of Sedimentology June 12–16, 2023, Dubrovnik, Croatia (field trip guidebook), 161–194.

Lyon C.H. & Molnar P. 1985: Gravity anomalies flexure of the Indian plate, and the structure, support and evolution of the Himalaya and Gangaa basin. *Tectonics* 4, 513–538. https://doi.org/10.1029/TC004i006p00513

Mandić O., de Leeuw A., Vuković B., Krijgsman W., Harzhauser M. & Kuiper K.F. 2011: Palaeoenvironmental evolution of Lake Gacko (Southern Bosnia and Herzegovina): Impact of the Middle Miocene Climatic Optimum on the Dinaride Lake System. *Palaeogeography, Palaeoclimatology, Palaeoecology* 299, 475–492. https://doi.org/10.1016/j.palaeo.2010.11.0124

Marroni M., Pandolfi L., Onuzzi K., Palandri S. & Xhomo A. 2009: Ophiolite-bearing Vermoshi flysch (Albanian Alps, Northern Albania): Elements for its correlation in the frame of Dinaric–Hellenic belt. *Ofioliti* 342, 95–108. https://doi.org/10.4454/ofioliti.v34i2.381

Márton E., Drobne K., Ćosović V. & Moro A. 2003: Palaeomagnetic evidence for Tertiary counterclockwise rotation of Adria. *Tectonophysics* 377, 143–156. https://doi.org/10.1016/j.tecto.2003.08.022

Matenco L. & Radivojević D. 2012: On the formation and evolution of the Pannonian Basin: Constraints derived from the structure of the junction area between the Carpathians and Dinarides. *Tectonics* 316, TC6007. https://doi.org/10.1029/2012TC003206

Matenco L., Krézsek C., Merten S., Schmid S., Cloetingh S. & Andriessen P. 2010: Characteristics of collisional orogens with low topographic build-up: an example from the Carpathians. *Terra Nova* 223, 155–165. https://doi.org/10.1111/j.1365-3121.2010.00931.x.

Mikes T., Christ D., Petri R., Dunkl I., Frei D., Báldi-Beke M., Reitner J., Wemmer K., Hrvatović H. & von Eynatten H. 2008: Provenance of the Bosnian Flysch. *Swiss Journal of Geosciences* 1, 31–54. https://doi.org/10.1007/s00015-008-1291-z

Mirković M., Kalezić P., Pajović M., Rašković S., Čepić M. & Vujičić P. 1980: Explanatory booklet for sheet Gacko. In: Basic Geological Map of Yugoslavia 1:100,000. *Federal Geological Institute*, Belgrade, 1–57.

Mrinjek E. 1993: Sedimentology and depositional setting of alluvial Promina beds in northern Dalmatia. *Geologia Croatica* 462, 243–261. https://doi.org/10.4154/GC.1993.22

Mudler T. & Alexander J. 2001: The physical character of subaqueous sedimentary density flows and their deposits. *Sedimentology* 48, 269–299. https://doi.org/10.1046/j.1365-3091.2001.00360.x

Neubauer F., Pamić J., Dunkl I., Handler R. & Majer V. 2003: Exotic granites in the Cretaceous Pogari Formation overstepping the Dinaric Ophiolite Zone mélange in Bosnia. *Annales Universitatis Scientarium Budapestinensis de Rolando Eötvös nominatae* 35, 133–134.

Olujić J. 1978: Distribution and genesis of Mesozoic flysches in Bosnia and Herzegovina. Unpublished Manuscript, Geological Survey of Bosnia and Herzegovina, Sarajevo.

Ortner H., Reiter F. & Acs P. 2002: Easy handling of tectonic data: the programs TectonicVB for Mac and TectonicsFP for Windows (TM). *Computers & Geosciences* 28, 1193–1200. https://doi.org/10.1016/S0098-3004(02)00038-9

Pamić J., Gušić I. & Jeleska V. 1998: Geodynamic evolution of the Central Dinarides. *Tectonophysics* 297, 251–268. https://doi.org/10.1016/S0040-1951(98)00171-1

Pamić J., Tomljenović B. & Balen D. 2002: Geodynamic and petrogenic evolution of Alpine ophiolites from the Central and NW Dinarides. *Lithos* 65, 113–142. https://doi.org/10.1016/S0024-4937(02)00162-7

Perch-Nielsen K. 1985: Cenozoic calcareous nannofossils. In: Bolli H.M., Saunders J.B. & Perch-Nielsen K. (eds.): Plankton stratigraphy. *Cambridge University Press*, 427–554.

Pinter N., Grenerczy G., Weber J., Stein S. & Medak D. 2005: The Adria Microplate: GPS Geodesy, Tectonics and Hazards. *Nato Science Series: IV: Earth and Environmental Sciences* 61, *Springer*, Dordrecht.

Poblet J. & Lisle R.J. 2011: Kinematic evolution and structural styles of fold and thrust belts. *Geological Society, London, Special Publications* 349, 1–24. https://doi.org/10.1144/SP349.1

Porkoláb K., Kövér S., Benkó Z., Héja H.G., Fialowski M., Soós B., Spajić G.N., Đerić N. & Fodor L. 2019: Structural and geochronological constraints from the Drina-Ivanjica thrust sheet (Western Serbia): implications for the Cretaceous–Paleogene tectonics of the Internal Dinarides. *Swiss Journal of Geosciences* 112, 217–234. https://doi.org/10.1007/s00015-018-0327-2

Rampnoux J.P. 1969: A propos du flysch du 'Durmitor' (Monténégro, Yougoslavie). *Compte rendu sommaire des séances de la Société géologique de France* 2, 54–55.

Rosenbaum G., Lister G.S. & Duboz C. 2002: Relative motions of Africa, Iberia and Europe during Alpine orogeny. *Tectonophysics* 359, 117–129. https://doi.org/10.1016/S0040-1951(02)00442-0

Šamarija R., Lužar B., Kukoč D., Kocjanić A., Gobo K., Petrinjak K. & Bjelogrlić M. 2025: Carbonate platform margin evolution in a compressive tectonic setting: an example from the Cretaceous of the Pre-Karst Unit of the Internal Dinarides (Gacko, Bosnia and Herzegovina). *Facies* 71, 9. https://doi.org/10.1007/s10347-025-00699-0

Schmid S., Bernoulli D., Fügenschuh B., Matenco L., Schefer S., Schuster R., Tischler M. & Ustaszewski K. 2008: The Alpine–Carpathian–Dinaridic orogenic system: Correlation and evolution of tectonic units. *Swiss Journal of Geosciences* 101, 139–183. https://doi.org/10.1007/s00015-008-1247-3

Schmid S., Fügenschuh B., Kounov A., Matenco L., Nievergelt P., Oberhansli R., Pleuger J., Schefer S., Schuster R., Tomljenović B., Ustaszeweski K. & van Hinsbergen D.J.J. 2020: Tectonic units of the Alpine collision zone between Eastern Alps and western Turkey. *Gondwana Research* 78, 343–346. https://doi.org/10.1016/j.gr.2019.07.005

Scilands 2015: The shaded hypsometric maps of Hungary, Slovakia, Slovenia, Croatia, Serbia, Bosnia & Herzegovina, Montenegro. Available online at: https://www.scilands.de/

Sinclair H.D. 1997a: Tectonostratigraphic model for underfilled peripheral foreland basins: An Alpine perspective. *GSA Bulletin* 109, 324–346. https://doi.org/10.1130/0016-7606(1997)109<0324:TMFUPF>2.3.CO;2

Sinclair H.D. 1997b: Flysch to molasse transition in peripheral foreland basins: The role of the passive margin versus slab breakoff. *Geology* 25, 1123–1126. https://doi.org/10.1130/0091-7613(1997)025<1123:FTMTIP>2.3.CO;2

Stampfli G.M. & Borel G.D. 2002: A plate tectonic model for the Paleozoic and Mesozoic constrained by dynamic plate boundaries and restored synthetic oceanic isochrones. *Earth and Planetary Science Letters* 196, 17–33. https://doi.org/10.1016/S0012-821X

Stojadinović U., Matenco L., Andriessen P., Toljić M., Rundić Lj. & Ducea M.N. 2017: Structure and provenance of Late Cretaceous–Miocene sediments located near the NE Dinarides margin: Inferences from kinematics of orogenic building and subsequent extensional collapse. *Tectonophysics* 710–711, 184–204. https://doi.org/10.1016/j.tecto.2016.12.021

Tavani S., Storti F., Lacombe O., Corradetti A., Mu˜noz, J.A. & Mazzoli S. 2015: A review of deformation pattern templates in foreland basin systems and fold-and thrust belts: Implications for the state of stress in the frontal regions of thrust Wedges. *Earth Science Reviews* 141, 82–104. https://doi.org/10.1016/j.earscirev.2014.11.013

Toljić M., Matenco L., Ducea M.N., Stojadinović U., Milivojević J. & Đerić N. 2013: The evolution of a key segment in the Europe–Adria collision: The Fruška Gora of northern Serbia. *Global and Planetary Change* 103, 39–62. https://doi.org/10.1016/j.gloplacha.2012.10.009

Toljić M., Matenco L., Stojadinović U., Willingshofer E. & Ljubović-Obradović D. 2018: Understanding fossil fore-arc basins: Inferences from the Cretaceous Adria–Europe convergence in the NE Dinarides. *Global and Planetary Change* 171, 167–184. https://doi.org/10.1016/j. gloplacha.2018.01.018

Ustaszewski K., Kounov A., Schmid S. M., Schaltegger U., Krenn E., Frank W. & Fügenschuh B. 2010: Evolution of the Adria-Europe plate boundary in the northern Dinarides: From continent-continent collision to back-arc extension. *Tectonics* 29, TC6017. https://doi.org/10.1029/2010TC002668

van Gelder I.E., Matenco L., Willingshofer E., Tomljenović B., Andriessen P.A.M., Ducea M.N. Beniest A. & Gruić A. 2015: The tectonic evolution of a critical segment of the Dinarides–Alps connection: Kinematic and geochronological inferences from the Medvednica Mountains, NE Croatia. *Tectonics* 34, 1952–1978. https://doi.org/10.1002/2015TC003937

van Unen M., Matenco L., Nader F.H., Darnault R., Mandić O. & Demir V. 2019: Kinematics of foreland-vergent crustal accretion: Inferences from the Dinarides evolution. *Tectonics* 38, 49–76. https://doi.org/10.1029/2018TC005066

Weber J., Vrabec M., Pavlovčič-Prešeren P., Dixon T., Jiang Y. & Stopar B. 2010: GPSderived motion of the Adriatic microplate from Istria Peninsula and Po Plain sites, and geodynamic implications. *Tectonophysics* 483, 214–222. https://doi.org/10.1016/j.tecto.2009.09.001

Žibret L. & Vrabec M. 2016: Paleostress and kinematic evolution of the orogen-parallel NW-SE striking faults in the NW External Dinarides of Slovenia unraveled by mesoscale fault-slip data analysis, *Geologia Croatica* 69, 295–305. https://doi.org/10.4154/gc.2016.30

Zupanić J. & Babić Lj. 2011: Sedimentary evolution of an inner foreland basin margin: Paleogene Promina Beds of the type area, Mt. Promina (Dinarides, Croatia). *Geologia Croatica* 64, 101–119. https://doi.org/10.4154/gc.2011.0

Electronic supplementary material is available online:
Supplementary Fig. S1 at https://geologicacarpathica.com/data/files/supplements/GC-77-1-Bjelogrlic_FigS1.jpg
Supplementary Fig. S2 at https://geologicacarpathica.com/data/files/supplements/GC-77-1-Bjelogrlic_FigS2.jpg
Supplementary Tables S1, S2 at https://geologicacarpathica.com/data/files/supplements/GC-77-1-Bjelogrlic_TableS1-S2.docx